

1
2
3
4
5
6
7
8
9
10
11
12
13
14
15
16
17
18
19
20
21
22
23

Developmental history modulates adult olfactory behavioral preferences via regulation of chemoreceptor expression in *C. elegans*

Travis Kyani-Rogers¹, Alison Philbrook¹, Ian G. McLachlan², Steven W. Flavell², Michael P. O'Donnell^{1,3} and Piali Sengupta^{1,4}

¹Department of Biology
Brandeis University
Waltham, MA 02454

²Picower Institute for Learning and Memory
Department of Brain and Cognitive Sciences
Massachusetts Institute of Technology
Cambridge, MA 02139

³Current address: Department of Molecular, Cellular and Developmental Biology, Yale University, New Haven, CT

⁴Corresponding author: sengupta@brandeis.edu

Running title: Developmental experience modulates adult olfactory behaviors

24 **ABSTRACT**

25 Developmental experiences play critical roles in shaping adult physiology and behavior.
26 We and others previously showed that adult *C. elegans* which transiently experienced dauer
27 arrest during development (PD: post-dauer) exhibit distinct gene expression profiles as compared
28 to control adults which bypassed the dauer stage. In particular, the expression patterns of subsets
29 of chemoreceptor genes are markedly altered in PD adults. Whether altered chemoreceptor levels
30 drive behavioral plasticity in PD adults is unknown. Here we show that PD adults exhibit
31 enhanced attraction to a panel of food-related attractive volatile odorants including the
32 bacterially-produced chemical diacetyl. Diacetyl-evoked responses in the AWA olfactory neuron
33 pair are increased in both dauer larvae and PD adults, and we find that these increased responses
34 are correlated with upregulation of the diacetyl receptor ODR-10 in AWA likely via both
35 transcriptional and post-transcriptional mechanisms. We show that transcriptional upregulation
36 of *odr-10* expression in dauer larvae is in part mediated by the DAF-16 FOXO transcription
37 factor. Via transcriptional profiling of sorted populations of AWA neurons from control and PD
38 adults, we further show that the expression of a subset of additional chemoreceptor genes in
39 AWA is regulated similarly to *odr-10* in PD animals. Our results suggest that developmental
40 experiences may be encoded at the level of olfactory receptor regulation, and provide a simple
41 mechanism by which *C. elegans* is able to precisely modulate its behavioral preferences as a
42 function of its current and past experiences.

43

44

45 INTRODUCTION

46 Conditions experienced during early development have profound effects on adult
47 phenotypes. Fetal malnutrition is a major risk factor for metabolic disorders in human adults, and
48 adverse experiences in early life influence adult stress responses in many animal species
49 (Alyamani and Murgatroyd, 2018; Cater and Majdic, 2021; de Gusmao Correia et al., 2012;
50 Hanson and Gluckman, 2014; Smith and Ryckman, 2015). In addition to modulating general life
51 history traits, early experiences can also affect specific adult behavioral phenotypes. For
52 instance, exposure to an odorant during a critical developmental period has been shown to
53 subsequently modulate the responses of adults to that odorant (Hong et al., 2017; Jin et al., 2016;
54 Nevitt et al., 1994; Remy and Hobert, 2005). Adult phenotypic plasticity as a consequence of
55 differential developmental experiences may allow adaptation to variable environments to
56 optimize fitness (Sommer, 2020). Despite the prevalence and critical role of early experiences in
57 shaping adult phenotypes, the underlying mechanisms are not fully understood.

58 *C. elegans* adults develop via one of two alternative developmental trajectories based on
59 environmental conditions experienced during their first and second larval stages (Cassada and
60 Russell, 1975). While larvae continue in the reproductive cycle through four larval stages (L1-
61 L4) under favorable conditions, adverse conditions experienced during L1 instead drive larvae
62 into the dauer diapause stage. Dauer larvae undergo extensive morphological, neuroanatomical
63 and behavioral remodeling that maximizes their ability to survive harsh conditions,
64 distinguishing them from their L3 larval counterparts (Albert and Riddle, 1983; Britz et al.,
65 2021; Popham and Webster, 1979; Riddle, 1988). When growth conditions improve, they exit
66 the dauer stage and resume development into reproductive adults. We and others previously
67 showed that adult *C. elegans* that transiently passed through the dauer stage (henceforth referred

68 to as post-dauer (PD) adults) differ markedly from adult animals that bypassed the dauer stage
69 (referred to as control adults) in their life history traits including longevity, stress-resistance, and
70 fecundity (Hall et al., 2010; Hall et al., 2013; Ow et al., 2018; Ow et al., 2021). This phenotypic
71 plasticity is correlated with extensive changes in transcriptional profiles, as well as modification
72 of the chromatin landscape (Bhattacharya et al., 2019; Hall et al., 2010; Hall et al., 2013; Ow et
73 al., 2018; Vidal et al., 2018). Thus, isogenic populations of adult *C. elegans* hermaphrodites
74 retain a molecular and phenotypic memory of their developmental history.

75 Food-seeking is a critical behavioral drive and is subject to extensive modulation as a
76 function of an animal's internal state and external conditions (Flavell et al., 2020; Heisler and
77 Lam, 2017; Kim et al., 2017; Pool and Scott, 2014). Dauer larvae do not feed and the
78 morphologies of their sensory neurons are extensively remodeled (Albert and Riddle, 1983; Britz
79 et al., 2021; Popham and Webster, 1979; Riddle, 1988). Dauer larvae retain the ability to detect
80 and respond to environmental cues including food-related chemical cues in order to assess
81 whether conditions have improved sufficiently to trigger exit from the dauer stage and re-entry
82 into the reproductive cycle. Chemosensory responses of *C. elegans* dauer larvae have been
83 assessed in a limited set of studies and appear to be partly distinct from those of adults or L3
84 larvae (Albert and Riddle, 1983; Hallem et al., 2011; Vertiz et al., 2021; White et al., 2019).
85 Whether PD adults retain these behavioral differences or exhibit further plasticity in food-
86 seeking behaviors as a consequence of their distinctive developmental trajectory is largely
87 unknown. The expression of many chemoreceptor genes in sensory neurons is altered in dauer
88 larvae (Nolan et al., 2002; Peckol et al., 2001; Vidal et al., 2018), and the spatial patterns and/or
89 levels of a subset of these genes is subsequently maintained or further altered in PD adults (Hall
90 et al., 2010; Peckol et al., 2001; Vidal et al., 2018). Altered chemoreceptor expression profiles

91 provide a plausible mechanism for chemosensory behavioral plasticity, but a correlation between
92 changes in chemoreceptor gene expression and altered food-seeking behaviors in PD animals
93 remains to be established.

94 Here we show that PD adults exhibit increased sensitivity to a panel of bacterially-
95 produced attractive odorants including the chemical diacetyl, low concentrations of which are
96 sensed by the AWA olfactory neuron pair. Consistently, both dauer larvae and PD adults also
97 exhibit increased diacetyl-evoked responses in the AWA olfactory neurons. We find that the
98 AWA-expressed *odr-10* diacetyl receptor gene is upregulated in dauer larvae; this upregulation is
99 mediated in part via the DAF-16 FOXO transcription factor. While *odr-10* expression is
100 subsequently downregulated in PD adults relative to levels in dauer larvae, levels of the ODR-10
101 receptor protein in the AWA cilium, the site of primary odorant transduction, are retained at
102 higher levels in PD as compared to control adults. Via transcriptional profiling of sorted
103 populations of AWA neurons from control and PD adults together with examination of
104 expression from endogenous reporter-tagged alleles, we further find that the expression of a
105 subset of additional AWA-expressed chemoreceptor genes is also upregulated in dauers, and is
106 maintained at higher levels in PD adults. Together, our data demonstrate that altered
107 chemoreceptor levels can underlie developmental stage- and history-dependent olfactory
108 behavioral plasticity in *C. elegans*, and highlight the complexity of mechanisms regulating
109 expression of individual chemoreceptor expression genes in this organism.

110

111 **MATERIALS and METHODS**

112 **Strains and growth conditions**

113 All *C. elegans* strains were maintained on nematode growth medium (NGM) seeded with
114 *Escherichia coli* OP50 at 20°C unless stated otherwise. Dauer larvae were generated by picking
115 8-10 L4s from continuously growing animal populations onto 10 cm NGM plates and allowing
116 growth and reproduction until food exhaustion (typically 7-9 days) at 25°C. Starved larvae were
117 washed off plates with S-Basal buffer, and dauer larvae were selected by treatment with 1% SDS
118 for 30 mins. To recover PD adults, a droplet containing 100-700 dauer larvae was pipetted onto a
119 10 cm NGM plate seeded with OP50 and allowed to grow for 48 hrs at 20°C. L4 larvae were
120 picked onto fresh, seeded NGM plates 1 day prior to imaging.

121 For all experiments involving growth on plates containing auxin, NGM media was
122 supplemented with the synthetic auxin 1mM 1-Naphthaleneacetic acid (NAA) from a 500 mM
123 stock solution dissolved in 95% ethanol. Corresponding control NGM media was supplemented
124 with an equal volume of 95% ethanol.

125 To collect adult animals that underwent L1 larval arrest, gravid adult hermaphrodites
126 were bleached, and eggs were allowed to hatch overnight in M9 buffer containing 0.1% Triton
127 X-100. 500-1000 L1 larvae were subsequently placed onto 10 cm NGM plates seeded with OP50
128 and grown at 20°C until adulthood.

129

130 **Genetics**

131 All strains were constructed using standard genetic methods. Crosses were validated for
132 the presence of the desired mutations using PCR-based amplification and/or sequencing. To
133 generate strains for auxin-induced degradation specifically in AWA, animals were injected with
134 a plasmid driving TIR1 under the AWA specific *gpa-4Δ6* promoter (PSAB1283: *gpa-*

135 *4Δ6p::TIR1::SL2::mScarlet*; Table S1) at 5 ng/μl together with the *unc-122p::dsRed* co-injection
136 marker at 50 ng/μl. A complete list of strains used in this work is available in Table S2.

137

138 **Molecular biology**

139 Gene editing was performed using CRISPR/Cas9 and repair templates. Plasmids
140 PSAB1279 (*odr-10::splitGFP₁₁*) and PSAB1280 (*gpa-4Δ6p::splitGFP₁₋₁₀*) (Table S1) were
141 generated using traditional cloning from splitGFP constructs (KP#3315 and KP#3316, gift from
142 J. Kaplan lab). An asymmetric donor template (Dokshin et al., 2018) was amplified from plasmid
143 PSAB1279 to create long and short PCR fragments of 2308 and 600 bp, respectively, containing
144 approximately 1 kb homology arms for CRISPR-mediated insertion. The asymmetric hybrid
145 template was injected (each fragment at 250 ng/μl) together with crRNA (20 ng/μl; IDT
146 Integrated DNA Technologies), tracrRNA (20 ng/μl; IDT), Cas9 protein (25 ng/μl; IDT), and
147 *unc-122p::gfp* (40 ng/μl) as the co-injection marker. F1 animals expressing the injection marker
148 were isolated. F2 progeny were screened by PCR for the insertion and confirmed by sequencing
149 to obtain *odr-10(oy158)* (Table S2).

150 To mutate the predicted DAF-16 binding site upstream of *odr-10* in *odr-10(oy158)*, a
151 conserved GTAAACA binding site 815 bp 5' of the *odr-10* start codon (Wexler et al., 2020) was
152 mutated to GTCCCCA to generate *odr-10(oy170)*. The injection mix contained an *odr-10*
153 promoter repair template with the mutated site along with 32 bp 5' and 3' homology arms (590
154 ng/μl; IDT), *dpy-10* repair template (100 ng/μl, IDT), Cas9 protein (25 ng/μl; IDT), crRNA (20
155 ng/μl; IDT), and tracrRNA mix (20 ng/μl; IDT). F1 animals with *dpy* phenotypes were isolated
156 and F1 and F2 progeny were screened by PCR and sequencing. Confirmed mutants were
157 backcrossed to remove the *dpy-10* allele.

158

159 **Chemotaxis behavioral assays**

160 Chemotaxis assays were performed essentially as described previously (Bargmann et al.,
161 1993; Troemel et al., 1997). Behavioral attraction and avoidance assays were performed on 10
162 cm round or square plates, respectively. Each assay was performed in duplicate each day, and
163 data are reported from biologically independent assays performed over at least 3 days. Behaviors
164 of control and experimental animals were examined in parallel each day.

165

166 **Calcium imaging**

167 Calcium imaging was performed essentially as previously described, using custom
168 microfluidics devices (Chronis et al., 2007; Khan et al., 2022; Neal et al., 2015). Imaging was
169 performed on an Olympus BX52WI microscope with a 40X oil objective and Hamamatsu Orca
170 CCD camera. Video recordings were performed at 4 Hz. All odorants were diluted in filtered S-
171 Basal buffer. 20 μ M fluorescein was added to one buffer channel to confirm correct fluid flow in
172 microfluidics devices. 1 mM (-)-tetramisole hydrochloride (Sigma L9756) was used to
173 immobilize animals during imaging. To prevent animals from clogging the microfluidics loading
174 arena and chip, 1 μ l of poloxamer surfactant (Sigma P5556) was added to the S-Basal loading
175 buffer. AWA neurons were imaged for one cycle of 30 sec buffer/30 sec odor/30 sec buffer, or
176 for one cycle of 30 sec buffer/10 sec odor/20 sec buffer stimuli.

177 Recorded images were aligned with the template Matching plugin in Fiji (NIH) and
178 cropped to include the AWA neuron soma and surrounding background fluorescence. The region
179 of interest (ROI) was defined by outlining the AWA cell bodies, and an area of background
180 fluorescence was chosen for background subtraction. To correct for photobleaching, an

181 exponential decay was fit to the fluorescence intensity values for the first 30 sec and the last 20
182 sec of imaging. The resulting value was subtracted from original intensity values. Peak
183 amplitude was calculated as the maximum change in fluorescence ($F-F_0$) in the 10 sec following
184 odor addition; F_0 was set to the average $\Delta F/F_0$ value for 5 sec before odor onset. Data
185 visualization was performed using RStudio (Version 1.4.1717). Photomask designs for
186 customized adult and dauer microfluidic imaging chips were adapted from (Chronis et al., 2007)
187 and are available at <https://github.com/SenguptaLab/PDplasticity> (also see below). AWA neuron
188 mean baseline fluorescence (Figure S1C) was calculated by taking the average $\Delta F/F_0$ during the
189 first 25 sec of imaging (0-25 sec) in each animal. Reported data were collected from biologically
190 independent experiments over at least 2 days.

191

192 **Dauer microfluidics imaging device**

193 Designs were based on olfactory imaging chips previously described (Chronis et al.,
194 2007) with modifications to accommodate dauer larvae. To constrict the thinner dauer larvae in a
195 similar manner to adults, it was necessary to reduce the cross-sectional area of the worm trap.
196 This was accomplished by placing 10 μm -wide posts of decreasing width culminating in a 5 μm
197 gap into which the worm nose was constricted (<https://github.com/SenguptaLab/PDplasticity>).
198 Posts were used instead of fully narrowing the channel to preclude limiting fluid velocity while
199 loading animals into the channel. AutoCAD drawings were used to generate an ink photomask
200 (outputcity.com) which was subsequently used to generate master molds with 10 μm feature
201 depth using negative photoresist SU-8 3005. To prevent delamination due to small features, a
202 uniform 10 μm layer of SU-8 3005 photoresist was applied first to silicon wafers.

203

204 **Imaging and image analysis**

205 Animals were mounted on 10% agarose pads set on microscope slides and immobilized
206 using 10 mM (-)-tetramisole hydrochloride. Imaging for expression level quantification was
207 performed on an inverted spinning disk confocal microscope (Zeiss Axiovert with a Yokogawa
208 CSU22 spinning disk confocal head and a Photometrics Quantum SC 512 camera). Optical
209 sections were acquired at 0.27 μ M sections using either a 63X oil immersion objective when
210 imaging neuron cell bodies, or a 100X oil immersion objective when imaging the cilia using
211 SlideBook 6.0 software (Intelligent Imaging Innovations, 3i). z-projections of all optical sections
212 at maximum intensity were generated using SlideBook 6.0 or FIJI/ImageJ (NIH).

213 Quantification of GFP or mNeonGreen levels in AWA soma was performed by tracing
214 the ROI of each neuron cell body, and subtracting background fluorescence. The mean
215 fluorescence of each cell body was calculated in FIJI. For quantification of ciliary ODR-10
216 levels in adult animals, an ROI of the cilia base and primary stalk was obtained and the
217 integrated density of total fluorescence in the ROI was calculated using the corrected total cell
218 fluorescence (CTCF) to take into account differences in the sizes of different ROIs and the
219 highly branched structures of AWA cilia. Since the AWA cilia branches are collapsed in dauer
220 larvae and are relatively smaller in L3 larvae, the ROI was traced around the entire cilia base and
221 stalks. Three background ROIs were obtained and averaged to calculate the mean background
222 fluorescence.

223

224 **Collection of AWA neurons**

225 To obtain control animals, adult hermaphrodites expressing the stably integrated
226 transgene *gpa-4Δ6p::myrGFP* (PY10421, Table S2) were bleached, and eggs allowed to hatch in

227 M9 with 0.1% Triton-100. 50,000-100,000 growth-synchronized L1 larvae were plated onto 15
228 cm 8P growth plates seeded with 1 ml of an overnight culture of *E. coli* NA22 grown in 2XYT
229 media. L1 larvae were allowed to grow for 40-48 hrs at 20°C to obtain populations of L4 larvae.
230 To obtain PD animals, SDS-selected dauer larvae were plated onto 15 cm 8P plates seeded with
231 1 ml of an overnight culture of *E. coli* NA22 grown in 2XYT media, and allowed to recover to
232 the L4 stage for 20-24 hrs at 20°C.

233 Animals were collected and cells dissociated essentially as described previously (Taylor
234 et al., 2021). In brief, animals were washed off plates with M9 buffer and incubated in lysis
235 buffer (200 mM Dithiothreitol (DTT), 0.25% Sodium dodecyl sulfate (SDS), 20 mM HEPES
236 buffer (4-(2-hydroxyethyl)-1-piperazineethanesulfonic acid), 3% sucrose) for 5 mins. Lysed
237 animals were washed 5X with egg buffer (118 mM NaCl, 48 mM KCl, 2 mM CaCl₂, 2 mM
238 MgCl₂, 25 mM HEPES, pH 7.3) following which the worm pellet was resuspended in 750 µl of
239 15 mg/ml Pronase (Sigma P8811) in egg buffer. To promote dissociation, the mixture was
240 pipetted frequently for 20 mins and progress of dissociation was monitored under a light
241 microscope. Pronase digestion was terminated by adding L-15-10 media (L-15 media + 10%
242 volume FBS, HI) at 4°C. Dissociated worms were centrifuged at 4°C and the worm pellet was
243 resuspended in egg buffer and recentrifuged at 4°C. The supernatant was filtered through a 35
244 µm filter in preparation for FACS sorting. A 25 µl aliquot of the dissociated worm pellet was
245 pipetted directly into Trizol for analysis as the whole worm sample.

246 Prior to performing FACS, 0.5 µl of 1 mg/ml DAPI was added to 1 ml of the cell
247 suspension to exclude dead cells. AWA neurons were captured by isolating the high GFP+ and
248 low DAPI compartment and cells were sorted directly into Trizol. Cells from this compartment
249 were also sorted onto glass slides and imaged under a fluorescence light microscope to confirm

250 the presence of intact GFP⁺ cells. Following cell collection, collection tubes were briefly spun
251 down and frozen at -80°C. 1,000 - 10,000 cells were isolated per sorting run.

252

253 **RNA sequencing**

254 RNA was extracted from collection tubes using standard chloroform and isopropanol
255 precipitation. The RNA pellet was resuspended in RNAase-free water and any DNA digested
256 using the RNase-Free DNase kit (Qiagen). RNA was eluted using the RNeasy MinElute Cleanup
257 Kit (Qiagen). mRNA was isolated and libraries amplified using Smart-Seq v4 and library quality
258 checked with Bioanalyzer using Agilent High Sensitivity Gel. Libraries were sequenced on
259 Illumina NextSeq500. Library preparation and sequencing was performed at the MIT BioMicro
260 Center (<https://biology.mit.edu/tile/biomicro-center/>).

261 Raw RNA-Seq reads were quality checked, adapter trimmed, and aligned to the *C.*
262 *elegans* genome using STAR ALIGNER (<https://github.com/alexdobin/STAR>). Principal
263 component analyses were performed on the normalized read counts of the 10,000 most variable
264 genes across all samples. Differential expression analysis was performed using DESeq2 with lfc
265 shrinkage on. Differential expression was determined with a significance cut-off of 0.05
266 (adjusted *p*-value; Wald test with Benjamini-Hochberg corrections) and the indicated Log₂ fold
267 change cut off of either -1.5 and 1.5 or -2 and 2. AWA enrichment analysis was performed using
268 the web-based Tissue Enrichment Analysis tool with default parameters
269 (<https://www.wormbase.org/tools/enrichment/tea/tea.cgi>) (Angeles-Albores et al., 2016).

270

271 **Statistical analyses**

272 Normal distribution of the data was assessed using the Shapiro-Wilks test (GraphPad
273 Prism v9.0.2). Parametric data were analyzed using a two-tailed Welch's t-test or ANOVA. Non-
274 parametric data were analyzed using a Mann-Whitney t-test or Kruskal-Wallis test across
275 multiple conditions. Post hoc corrections for multiple comparisons were applied to data in which
276 more than two groups were analyzed. The specific tests used and corrections applied are
277 indicated in each Figure Legend.

278

279 **RESULTS**

280 **Post-dauer adult animals exhibit enhanced attraction to a subset of volatile odorants**

281 *C. elegans* adult animals are strongly attracted to a subset of chemicals that indicates the
282 presence of nutritious bacteria, the major food source for these nematodes (Ferkey et al., 2021).
283 Attractive volatile odorants are primarily sensed by the AWA and AWC olfactory neurons pairs
284 in the bilateral head amphid organs of *C. elegans* (Bargmann et al., 1993). Consistently, adult
285 hermaphrodite animals grown continuously under favorable environmental conditions (control
286 adults; Figure 1A) exhibited robust attraction to a range of concentrations of odorants sensed by
287 the AWA and/or AWC neurons (Figure 1B).

288 To test whether passage through the dauer stage influences the olfactory preference
289 behaviors of adult animals, we grew wild-type animals under food-restricted conditions to
290 promote entry into the dauer stage as previously described (Figure 1A) (Ow et al., 2018). Dauer
291 larvae were collected via SDS-mediated selection and subsequently allowed to resume
292 reproductive growth on bacterial food (Figure 1A). Similar to control adults, young post-dauer
293 (henceforth referred to as PD) adult animals were also robustly attracted to both AWA- and
294 AWC-sensed volatile odorants (Figure 1B). We found that PD adults typically exhibited

295 enhanced attraction to lower odorant concentrations relative to control adults (Figure 1B).
296 Animals that experienced starvation-induced developmental arrest at the L1 larval stage did not
297 exhibit similar enhanced attraction responses as adults (Figure S1A). PD animals have
298 previously been shown to exhibit decreased avoidance of the aversive pheromone *ascr#3* (Sims
299 et al., 2016). Control and PD animals avoided high concentrations of benzaldehyde to a similar
300 extent (Figure S1B) although the aversion responses of PD adults to high concentrations of
301 octanol were weakly decreased (Figure S1B). We conclude that the behavioral responses of adult
302 animals to multiple attractive volatile chemicals are sensitized upon passage through the dauer
303 diapause stage.

304 We next tested whether increased behavioral attraction correlates with enhanced odorant
305 responses in olfactory neurons by examining odorant-evoked changes in intraneuronal calcium
306 dynamics using a genetically encoded calcium indicator. We focused our attention on the odorant
307 diacetyl, low concentrations of which are sensed by the AWA olfactory neuron pair (Bargmann
308 et al., 1993), and for which the cognate receptor and signal transduction mechanisms have been
309 described (see below) (Colbert et al., 1997; Roayaie et al., 1998; Sengupta et al., 1996). Low
310 concentrations of diacetyl consistently evoked responses of larger amplitude in the AWA
311 neurons of PD as compared to control adults consistent with the observed increased behavioral
312 responses to this chemical (Figure 1C-D). This amplitude difference is unlikely to arise simply
313 due to differences in the expression levels of the AWA-expressed calcium sensor (Figure S1C).
314 Together, these data indicate that neuronal responses of adult animals to the attractant diacetyl
315 are enhanced upon passage through the dauer stage.

316

317 **Ciliary levels of the diacetyl receptor ODR-10 are increased as a function of developmental**
318 **history**

319 We and others previously reported that control and PD animals exhibit significant
320 differences in gene expression profiles including in individual sensory neurons (Bhattacharya et
321 al., 2019; Hall et al., 2010; Sims et al., 2016; Vidal et al., 2018). Each chemosensory neuron type
322 in *C. elegans* expresses multiple GPCRs, expression of a subset of which has previously been
323 shown to be regulated by external and internal state (Gruner et al., 2014; Lanjuin and Sengupta,
324 2002; Nolan et al., 2002; Peckol et al., 2001; Ryan et al., 2014; Troemel et al., 1995; Vidal et al.,
325 2018). Low concentrations of diacetyl are sensed by the ODR-10 olfactory receptor which is
326 expressed specifically in the AWA neurons and localizes to their sensory cilia, the primary site
327 of olfactory signal transduction (Sengupta et al., 1996). Behavioral and neuronal responses to
328 diacetyl have previously been shown to be regulated by feeding state, developmental stage and
329 somatic sex via expression changes in *odr-10* (Ryan et al., 2014; Wexler et al., 2020), but
330 whether *odr-10* expression is also modulated via dauer passage is unclear. Since state-dependent
331 regulation of individual olfactory receptor genes provides a simple mechanism for mediating
332 odorant-selective behavioral plasticity, we tested the hypothesis that altered expression of *odr-10*
333 underlies the observed plasticity in diacetyl responses in PD adults.

334 An endogenous *odr-10* allele tagged with *t2A::mNeonGreen* (*odr-10::t2A::mNG*) was
335 specifically expressed in both AWA neurons (Figure 2A) (McLachlan et al., 2022). However,
336 expression levels of the fluorescent reporter protein were not significantly altered in PD as
337 compared to control adults (Figure 2B). Since this reporter does not allow assessment of ciliary
338 ODR-10 protein levels, we next quantified ODR-10 protein levels in AWA cilia from the
339 endogenous *odr-10* allele tagged with the split-GFP reporter GFP₁₁ (*odr-10(oy158)*), and

340 reconstitution of GFP via expression of the GFP₁₋₁₀ fragment under a constitutive AWA-specific
341 promoter (Kamiyama et al., 2016). We confirmed that tagging *odr-10* with GFP₁₁ had no effect
342 on behavioral responses to diacetyl, and that these animals continued to exhibit enhanced
343 attraction to diacetyl upon passage through the dauer stage (Figure S2A). The reconstituted
344 ODR-10 fusion protein was localized to the extensively branched AWA cilia in both control and
345 PD animals (Figure 2C). Since the complex architecture of the AWA cilium precluded precise
346 quantification of overall ciliary protein levels in adult animals, we restricted our analysis to
347 assessing ODR-10 protein levels at the ciliary base and in the primary ciliary stalk. We found
348 that reconstituted ODR-10::GFP levels in AWA cilia were significantly higher in PD than in
349 control animals (Figure 2C-D). These observations raise the possibility that increased ciliary
350 levels of ODR-10 protein in PD animals may contribute to the increased diacetyl responses of
351 PD animals.

352 To establish whether increasing ODR-10 levels alone in AWA is sufficient to enhance
353 diacetyl response sensitivity even in control animals, we overexpressed *odr-10* from the
354 constitutive *gpa-4Δ6* promoter and examined diacetyl responses via both behavioral assays and
355 imaging of diacetyl-evoked intracellular calcium dynamics. As shown in Figure 2E, the
356 behavioral responses of control animals overexpressing *odr-10* were higher than those of wild-
357 type control animals across multiple concentrations of diacetyl. Overexpression of *odr-10* was
358 also sufficient to increase diacetyl-evoked calcium responses in AWA in control adults (Figure
359 2F, Figure S2B). We conclude that increased ODR-10 levels may be sufficient to account for the
360 enhanced diacetyl responses of PD animals.

361

362 ***odr-10* expression and diacetyl behavioral responses are increased in dauer larvae**

363 *C. elegans* dauer larvae as well as the analogous infective juvenile larvae of parasitic
364 nematodes have been shown to exhibit distinct olfactory behaviors (Vertiz et al., 2021). The
365 expression of many neuronal genes including chemoreceptor genes is also markedly altered in
366 dauer larvae (Bhattacharya et al., 2019; Hall et al., 2010; Nolan et al., 2002; Peckol et al., 2001;
367 Vidal et al., 2018). The dauer-specific expression patterns of a subset of these genes is
368 maintained in PD adults, while the expression of other genes is further altered to a PD-specific
369 pattern or restored to the pattern observed in control adults (Hall et al., 2010; Peckol et al., 2001;
370 Vidal et al., 2018). We asked whether *odr-10* expression is modulated in dauers, following which
371 ciliary protein levels may be subsequently maintained at higher levels in PD animals.

372 Expression of the *odr-10::t2A::mNG* reporter remained restricted to the AWA neurons in
373 dauer larvae (Figure 3A). In contrast to our observations in PD adults, *odr-10::t2A::mNG*
374 expression was strongly upregulated in dauer animals as compared to levels in L3 larvae (Figure
375 3A-B). Consistently, reconstituted ODR-10::GFP protein levels were also increased in AWA
376 cilia in dauers (Figure 3C-D).

377 We tested whether upregulation of *odr-10* expression in dauers correlates with increased
378 diacetyl responses in these animals. To examine diacetyl-evoked calcium responses in AWA, we
379 modified the microfluidics imaging device typically used for imaging *C. elegans* adults (Chronis
380 et al., 2007) to accommodate the thinner and smaller dauer larvae (see Materials and Methods),
381 although we were unable to use these or the adult imaging devices to examine L3 larvae. In
382 response to a pulse of 10^{-5} dilution of diacetyl, dauer animals exhibited markedly increased
383 responses as compared to control or PD adults (Figure 3E-F). Altered expression levels of the
384 calcium sensor in AWA are unlikely to account for the observed increase in diacetyl responses in
385 dauer larvae (Figure S1C). We could not reliably assess the behavioral responses of dauers to

386 diacetyl in our behavioral assays in part due to their unique locomotory patterns (Bhattacharya et
387 al., 2019; Gaglia and Kenyon, 2009), although we note that a previous report indicated that
388 dauers exhibit decreased behavioral responses to diacetyl (Vertiz et al., 2021). We conclude that
389 *odr-10* may be upregulated upon entry into the dauer stage possibly via transcriptional
390 mechanisms and correlates with increased diacetyl responses. While this transcriptional
391 upregulation is not maintained in PD adults, increased ODR-10 protein levels in AWA cilia
392 correlates with enhanced diacetyl responses in PD adults.

393

394 **Upregulation of *odr-10* expression in dauer larvae is mediated in part via the DAF-16**
395 **FOXO transcription factor**

396 The TGF- β and insulin signaling pathways act in parallel to regulate dauer formation in
397 response to adverse environmental conditions (Fielenbach and Antebi, 2008; Riddle and Albert,
398 1997). Insulin signaling inhibits nuclear translocation of the DAF-16 FOXO transcription factor,
399 and DAF-16 is nuclear-localized in dauer larvae (Aghayeva et al., 2021; Lin et al., 1997; Ogg et
400 al., 1997). Since this molecule has been implicated in the altered regulation of sensory gene
401 expression in dauer larvae (Aghayeva et al., 2021; Bhattacharya et al., 2019; Wexler et al.,
402 2020), we tested whether the observed upregulation of *odr-10* expression in dauers is mediated
403 in part via DAF-16-dependent transcriptional regulation.

404 Since *daf-16* mutants cannot enter the dauer stage, we assessed the effects of *daf-16*
405 depletion via auxin-induced degradation specifically in AWA (Nishimura et al., 2009; Zhang et
406 al., 2015). We expressed the auxin receptor TIR1 in AWA in a strain in which the endogenous
407 *daf-16* locus has been edited to include a degron tag (Aghayeva et al., 2020; Aghayeva et al.,
408 2021). To obtain larger numbers of dauer larvae, these experiments were performed in *daf-2*

409 insulin receptor mutants that constitutively enter the dauer stage even under favorable
410 environmental conditions (Figure 4A) (Gems et al., 1998; Riddle et al., 1981). As in wild-type
411 animals, *odr-10::t2A::mNG* expression levels were upregulated in *daf-2* dauer larvae as
412 compared to expression levels in control or PD *daf-2* adults in the absence of auxin treatment
413 (Figure 4B). We found that auxin-mediated depletion of DAF-16 in AWA decreased, although
414 did not fully abolish, the upregulated *odr-10* expression observed in dauer animals (Figure 4Ai,
415 4B). Growth on auxin had little effect on *odr-10* expression levels in adult animals that bypassed
416 the dauer stage (Figure 4Aii, 4B), although we note that *odr-10* was previously identified as a
417 putative DAF-16-regulated gene in a comparison of the neuronal transcriptomes of *daf-2* and
418 *daf-16*; *daf-2* adult animals (Kaletsky et al., 2015). Addition of auxin only during dauer recovery
419 also did not affect *odr-10* expression in adult animals (Figure 4Aiii, 4B). We infer that DAF-
420 function in AWA is partly necessary during dauer entry to transcriptionally upregulate *odr-10*
421 expression, although we are unable to exclude the possibility that DAF-16 is not fully depleted in
422 AWA under these conditions.

423 A putative DAF-16 binding site in the proximal regulatory sequences of *odr-10* was
424 previously shown to be necessary for starvation-dependent upregulation of *odr-10* expression
425 driven from a transcriptional reporter in *C. elegans* males (Wexler et al., 2020). In contrast to the
426 expression of the endogenous *odr-10::t2A::mNG* reporter, transgenic expression of GFP driven
427 by ~1kb of the *odr-10* promoter containing the predicted DAF-16 binding site retained high
428 levels of expression in PD adults (Figure 4C). Mutating the predicted DAF-16 binding site in this
429 reporter construct decreased expression levels in PD adults (Figure 4C). However, mutating this
430 site in the endogenous *odr-10* locus via gene editing had no effect on the upregulated levels of
431 ciliary ODR-10 protein in either dauer or PD animals (Figure 4D). These results suggest that

432 multiple DAF-16 binding sites in *odr-10* regulatory sequences may contribute redundantly in the
433 context of the endogenous promoter to the upregulation of *odr-10* expression in dauer larvae.
434 Alternatively, DAF-16 may act indirectly to regulate endogenous *odr-10* expression.

435

436 **AWA neurons exhibit distinct gene expression profiles in control and PD adults**

437 In addition to diacetyl, PD adults also exhibit increased responses to the AWA-sensed
438 odorants pyrazine and 2,4,5-trimethylthiazole (Figure 1B). Although the receptors for these
439 chemicals are as yet unidentified, this observation suggests that the expression of
440 chemoreceptors in addition to *odr-10* in AWA may also be altered as a function of dauer
441 passage. To test this notion, we dissociated control and PD L4 larvae expressing GFP
442 specifically in AWA, collected GFP-labeled populations of AWA neurons via fluorescence-
443 activated cell sorting (FACS), and performed transcriptional profiling (Taylor et al., 2021). In
444 order to obtain large populations of growth-synchronized L4 animals for cell sorting, the control
445 population was grown from L1-arrested larvae (see Materials and Methods). In parallel, we also
446 transcriptionally profiled populations of dissociated but unsorted cells from control and PD L4
447 animals.

448 Principal component analyses indicated that with the exception of one sample, the RNA-
449 Seq profiles of all biologically independent replicates of sorted control and PD AWA neurons
450 were present in a cluster distinct from that obtained from cells collected from whole animals
451 (Figure S3A). AWA-expressed genes were the most enriched in the dataset collected from sorted
452 AWA neurons (Figure S3B). Moreover, the 20 most highly expressed genes in AWA as
453 predicted by the CeNGEN neuronal profiling project (Taylor et al., 2021) were robustly
454 represented as upregulated in the AWA RNA-Seq data as compared to data from whole animals

455 (Figure S3C). These observations indicate that we successfully enriched and profiled populations
456 of AWA neurons.

457 Comparison of the gene expression changes in the datasets from control and PD whole
458 animals indicated that the expression of multiple G protein-coupled receptor (GPCR) genes was
459 altered as a function of dauer passage (Figure 5A-B, File S1). There was minimal overlap with
460 previously published datasets of genes differentially regulated in PD vs control whole animals
461 (Hall et al., 2010; Ow et al., 2018), likely due to differences in conditions of animal growth and
462 sample preparation although we note that genes predicted to be involved in GPCR signaling were
463 also previously identified as a differentially expressed category (Hall et al., 2010). Up- or
464 downregulated chemoreceptor genes are predicted to be expressed in multiple chemosensory
465 neuron types, indicating that modulation of chemoreceptor gene expression as a function of
466 developmental history is mediated at the level of individual chemoreceptor genes and not
467 sensory neuron types. However, despite the established importance of neuropeptide and
468 hormonal signaling in regulating dauer entry (Fielenbach and Antebi, 2008; Riddle and Albert,
469 1997), the expression of only a few predicted neuropeptide genes appeared to be altered in PD as
470 compared to control animals (Figure 5B, File S1).

471 In contrast to the gene expression changes in the whole animal dataset, the expression of
472 only a small number of GPCRs appeared to be altered in PD vs control AWA neurons (Figure
473 5C-D, File S2). As expected, *odr-10* transcript levels were not significantly changed in PD
474 adults. However, we noted that the expression of several neuropeptide genes and in particular,
475 multiple transcription factors was significantly altered in PD vs control adults (Figure 5D, File
476 S2). Affected transcription factors belong to multiple subfamilies including the greatly expanded
477 nuclear hormone receptor family, members of which are predicted to be co-expressed in sensory

478 neurons along with putative chemoreceptor GPCRs, and which have been suggested to act as
479 receptors for external and internal cues (Sural and Hobert, 2021; Taylor et al., 2021). Together,
480 these results indicate that passage through the dauer stage alters the expression of genes from
481 multiple families, and that the expression of genes in individual sensory neurons such as AWA is
482 also affected.

483

484 **The expression of multiple AWA-expressed chemoreceptor genes is upregulated in dauers**
485 **and is maintained at higher levels in PD adults**

486 As described above, while *odr-10* expression is not altered in PD adults, expression of
487 this gene is transcriptionally upregulated in dauer larvae following which ciliary ODR-10::GFP
488 protein levels are maintained at higher levels in PD adults. Since our RNA-Seq experiments
489 indicated that the mRNA levels of only a small number of GPCR genes are altered in PD as
490 compared to control AWA neurons, we tested whether additional AWA-expressed
491 chemoreceptor genes are regulated similarly to *odr-10*.

492 Since we were unable to efficiently dissociate dauer larvae likely due to their modified
493 cuticle (Cassada and Russell, 1975) and thus could not profile populations of sorted AWA
494 neurons from dauer larvae, we instead examined the expression of a subset of endogenously
495 tagged chemoreceptor genes. Similar to *odr-10*, mRNA levels of the putative AWA-expressed
496 chemoreceptors *srd-27*, *srd-28*, and *str-44* were also not significantly upregulated in AWA in PD
497 adults (Figure 5C-D, File S2) although *srd-28* was identified as a gene upregulated in PD adults
498 in the whole animal dataset (Figure 5B). *srd-27*, *srd-28* and *str-44* endogenously tagged with
499 *t2A::mNG* were specifically expressed bilaterally in the AWA olfactory neurons in L3 larvae and
500 control adults (Figure 6A) (McLachlan et al., 2022). Expression of all three genes was

501 upregulated in AWA in dauer larvae as compared to L3 larvae with *srd-28* and *str-44* showing
502 stronger changes (Figure 6A-D). However, unlike *odr-10* whose expression remained restricted
503 to AWA in all examined stages, all three chemoreceptor genes were expressed in additional
504 neurons in the head in dauer larvae (Figure 6A). Expression in all neurons including in AWA
505 was subsequently downregulated in PD adults relative to dauer larvae, although *srd-28*, *str-44*,
506 and *srd-27* retained higher expression levels in PD as compared to control adults (Figure 6A-D).
507 As in the case of *odr-10*, depletion of DAF-16 during dauer entry via auxin-induced degradation
508 (Figure 4Ai) also decreased but did not abolish upregulation of *srd-28::t2A::mNG* expression in
509 dauer larvae (Figure 6E). We conclude that the expression of multiple AWA-expressed
510 chemoreceptor genes is likely transcriptionally upregulated in dauer larvae in part via DAF-16-
511 dependent mechanisms, and that increased levels of a subset of these receptors may be
512 maintained in PD adults possibly via non-transcriptional mechanisms.

513

514 **DISCUSSION**

515 We show here that adult *C. elegans* hermaphrodites that transiently passed through the
516 dauer developmental stage exhibit enhanced olfactory responses associated with food-seeking as
517 compared to adult animals that bypassed this stage. Increased sensitivity to the odorant diacetyl
518 is correlated with upregulated expression of the diacetyl receptor ODR-10 in dauer larvae, and
519 higher levels of the ODR-10 protein in AWA olfactory cilia in PD adults. Via transcriptional
520 profiling, we further show that levels of a subset of additional AWA-expressed chemoreceptors
521 are also modulated by developmental stage and trajectory. Our results suggest that state- and
522 experience-dependent cues are integrated to differentially modulate individual chemoreceptor
523 levels in a single sensory neuron type likely via both transcriptional and post-transcriptional

524 mechanisms, thereby providing a possible mechanism underlying developmental history-
525 dependent olfactory behavioral plasticity.

526 Upon entry into the dauer stage, *odr-10* expression is transcriptionally upregulated in part
527 via DAF-16. However, activation of DAF-16 alone appears to be insufficient to upregulate *odr-*
528 *10* expression since *odr-10* expression is not upregulated in *daf-2* insulin receptor mutants that
529 did not enter the dauer stage. Although we are unable to exclude the possibility that DAF-16 is
530 only partially depleted in AWA upon auxin treatment, it is likely that additional factors including
531 transcription factors such as the DAF-3 SMAD or the DAF-12 nuclear hormone receptor that act
532 downstream of dauer-promoting hormonal signals also play a role in regulating *odr-10*
533 expression (Aghayeva et al., 2021; Fielenbach and Antebi, 2008; Sims et al., 2016). Similarly,
534 altered expression of innexins and other chemoreceptors in dauers were shown to be only partly
535 DAF-16-dependent (Aghayeva et al., 2021). Upon exit from the dauer stage, *odr-10* expression
536 is downregulated possibly due to inactivation of DAF-16 and the altered chromatin profile of
537 these animals (Hall et al., 2010; Sims et al., 2016), but levels of ciliary ODR-10 protein continue
538 to be maintained at higher levels than in control animals. Ciliary GPCRs are trafficked to the
539 cilia base and further trafficked into and out of the cilium via diffusion and motor-driven
540 transport (Mukhopadhyay et al., 2017; Nachury and Mick, 2019). We previously showed that
541 ciliary trafficking of chemoreceptors in different *C. elegans* sensory neurons is regulated by
542 multiple neuron- and receptor-specific mechanisms, and that these trafficking mechanisms are
543 further modulated by sensory signaling (Brear et al., 2014; DiTirro et al., 2019). Sensory neuron
544 cilia including those of AWA are extensively remodeled in dauers but their morphologies appear
545 to be restored to those resembling those in control animals in PD adults (Albert and Riddle,
546 1983; Britz et al., 2021) (this work). We propose that one or more ciliary trafficking mechanisms

547 are altered in PD animals resulting in increased ODR-10 protein trafficking into, or decreased
548 removal from, the AWA cilia in PD animals. In addition to transcriptional changes in
549 chemoreceptor expression, regulated trafficking of ciliary GPCRs provides an additional
550 mechanism to fine tune sensory responses as a consequence of developmental experience.

551 Why do PD adults enhance their responses to food-related odors? Stress, including
552 starvation, experienced during early larval stages may indicate that food availability is unreliable.
553 Increased attraction to food in PD adults may be a bet-hedging strategy that optimizes growth
554 and survival in a variable environment. However, although animals also retain a cellular memory
555 of starvation-induced L1 arrest (Jobson et al., 2015; Webster et al., 2018), this arrest does not
556 appear to alter examined olfactory behaviors in adults, suggesting that stress assessed during a
557 distinct period in development and/or dauer entry is required to drive behavioral plasticity in
558 ensuing adults. Interestingly, we and others previously showed that expression of the *osm-9*
559 TRPV channel gene is strongly downregulated in the ADL nociceptive but not AWA neurons in
560 PD adults, resulting in decreased responses to the ADL-sensed aversive *ascr#3* pheromone (Sims
561 et al., 2016). Decreased aversion to this pheromone by PD adults has been suggested to be a
562 mechanism that inhibits dispersion in a crowded environment and promotes outcrossing (Sims et
563 al., 2016). Coordinated differential modulation of responses in defined subsets of chemosensory
564 neurons likely allow PD adults to optimize survival and reproduction.

565 In contrast to the main olfactory systems of vertebrates in which each olfactory sensory
566 neuron expresses one or very few olfactory receptors (Chess et al., 1994; Ressler et al., 1993;
567 Vassar et al., 1993), the co-expression of as many as 100 chemoreceptors in each chemosensory
568 neuron type in *C. elegans* (Taylor et al., 2021; Troemel et al., 1995; Vidal et al., 2018) raises a
569 unique challenge for this organism. Since co-expressed chemoreceptors are likely tuned to

570 distinct odorants, modulating synaptic transmission from a single chemosensory neuron in *C.*
571 *elegans* as a function of internal state would be expected to coordinately alter responses to a
572 broad range of chemicals sensed by that neuron type. Regulation of individual chemoreceptors
573 instead enables the animal to precisely target and modulate defined chemosensory behaviors.
574 Consistent with this notion, expression of chemoreceptor genes is subject to complex modes of
575 regulation. *odr-10* expression is higher in hermaphrodites and juvenile male larvae than in adult
576 males, and expression is upregulated in adults of both sexes upon starvation (Ryan et al., 2014;
577 Wexler et al., 2020). The expression of multiple chemoreceptors in many sensory neuron types is
578 dramatically altered in dauer larvae and subsequently further modulated in PD animals, whereas
579 the expression of other receptors is sexually dimorphic (Nolan et al., 2002; Peckol et al., 1999;
580 Troemel et al., 1995; Vidal et al., 2018). In the ADL nociceptive neurons, expression of the *srh-*
581 *234* chemoreceptor has been shown to be regulated via cell-autonomous and non cell-
582 autonomous mechanisms (Gruner et al., 2016; Gruner et al., 2014). Thus, the expression of each
583 chemoreceptor gene may be modulated by multiple regulatory modules that act combinatorially
584 to integrate distinct inputs and appropriately calibrate the behavioral response.

585 Individual chemosensory neurons in *Aedes aegypti* also express multiple receptors from
586 different receptor subfamilies (Younger et al., 2020). The expression of subsets of these
587 receptors has been shown to be modulated by feeding and reproductive state although whether
588 receptor expression is causative to altered olfactory behavioral profiles is unclear (Matthews et
589 al., 2016). In rodents, a subset of specialized olfactory neurons in rodents express multiple
590 receptors of the MS4A family, each of which responds to ethologically relevant chemical stimuli
591 (Greer et al., 2016). It will be interesting to assess whether expression of these receptors is also

592 subject to extensive state-dependent modulation, and whether this modulation drives sensory
593 behavioral plasticity as a function of current and past external and internal conditions.
594

595 **DATA AVAILABILITY STATEMENT**

596 All plasmids used in this work are listed in Table S1. All strains used in this work are
597 listed in Table S2. Strains and plasmids are available upon request. Data underlying this article
598 are available at <https://github.com/SenguptaLab/PDplasticity>. Sequencing files of the RNA-Seq
599 experiments have been deposited in the Array Express database at EMBL-EBI
600 (www.ebi.ac.uk/arrayexpress) under accession number E-MTAB-11823.

601

602 **ACKNOWLEDGEMENTS**

603 We thank Oliver Hobert and Mario de Bono for reagents and experimental advice, David
604 Miller, Nicolas Henderson and Dylan Ma for assistance with cell sorting, Albert Yu and Ines
605 Patop for assistance with analyses of RNA-Seq data, Bradly Stone for assistance with statistical
606 analyses, and the *Caenorhabditis* Genetics Center for strains. We are grateful to members of the
607 Sengupta lab for advice and members of the Sengupta lab, Doug Portman and Sarah Hall for
608 critical comments on the manuscript.

609

610 **FUNDING**

611 This work was supported in part by the National Science Foundation (IOS 165518 and
612 IOS 2042100 – P.S., IOS 1845663 – S.W.F., DMR 2011846 – Brandeis Materials Research
613 Science and Engineering Center), the National Institutes of Health (F32 DC018453 – A.P., R35
614 GM122463 – P.S., R01 NS 104892 – S.W.F.) the JPB Foundation (S.W.F.), the McKnight
615 Foundation (S.W.F.), and the Alfred P. Sloan Foundation (S.W.F.).

616

617 **REFERENCES**

- 618 Aghayeva, U., Bhattacharya, A., and Hobert, O. (2020). A panel of fluorophore-tagged *daf-16*
619 alleles. *Micropub. Biol.* 10.17912/micropub.biology.000210.
- 620 Aghayeva, U., Bhattacharya, A., Sural, S., Jaeger, E., Churgin, M., Fang-Yen, C., and Hobert, O.
621 (2021). DAF-16/FoxO and DAF-12/VDR control cellular plasticity both cell-autonomously
622 and via interorgan signaling. *PLoS Biol* 19, e3001204.
- 623 Albert, P.S., and Riddle, D.L. (1983). Developmental alterations in sensory neuroanatomy of the
624 *Caenorhabditis elegans* dauer larva. *J Comp Neurol* 219, 461-481.
- 625 Alyamani, R.A.S., and Murgatroyd, C. (2018). Epigenetic programming by early-life stress. *Prog*
626 *Mol Biol Transl Sci* 157, 133-150.
- 627 Angeles-Albores, D., RY, N.L., Chan, J., and Sternberg, P.W. (2016). Tissue enrichment
628 analysis for *C. elegans* genomics. *BMC Bioinformatics* 17, 366.
- 629 Bargmann, C.I., Hartwig, E., and Horvitz, H.R. (1993). Odorant-selective genes and neurons
630 mediate olfaction in *C. elegans*. *Cell* 74, 515-527.
- 631 Bhattacharya, A., Aghayeva, U., Berghoff, E.G., and Hobert, O. (2019). Plasticity of the
632 electrical connectome of *C. elegans*. *Cell* 176, 1174-1189 e1116.
- 633 Brear, A.G., Yoon, J., Wojtyniak, M., and Sengupta, P. (2014). Diverse cell type-specific
634 mechanisms localize G protein-coupled receptors to *C. elegans* sensory cilia. *Genetics* 197,
635 667-684.
- 636 Britz, S., Markert, S.M., Witvliet, D., Steyer, A.M., Troger, S., Mulcahy, B., Kollmannsberger,
637 P., Schwab, Y., Zhen, M., and Stigloher, C. (2021). Structural analysis of the
638 *Caenorhabditis elegans* dauer larval anterior sensilla by focused ion beam-scanning
639 electron microscopy. *Front Neuroanat* 15, 732520.
- 640 Cassada, R.C., and Russell, R.L. (1975). The dauer larva, a post-embryonic developmental
641 variant of the nematode *Caenorhabditis elegans*. *Dev Biol* 46, 326-342.
- 642 Cater, M., and Majdic, G. (2021). How early maternal deprivation changes the brain and
643 behavior? *Eur J Neurosci* 55, 2058-2075.
- 644 Chess, A., Simon, I., Cedar, H., and Axel, R. (1994). Allelic inactivation regulates olfactory
645 receptor gene expression. *Cell* 78, 823-834.
- 646 Chronis, N., Zimmer, M., and Bargmann, C.I. (2007). Microfluidics for *in vivo* imaging of
647 neuronal and behavioral activity in *Caenorhabditis elegans*. *Nat Methods* 4, 727-731.
- 648 Colbert, H.A., Smith, T.L., and Bargmann, C.I. (1997). OSM-9, a novel protein with structural
649 similarity to channels, is required for olfaction, mechanosensation, and olfactory adaptation
650 in *Caenorhabditis elegans*. *J Neurosci* 17, 8259-8269.
- 651 de Gusmao Correia, M.L., Volpato, A.M., Aguila, M.B., and Mandarim-de-Lacerda, C.A.
652 (2012). Developmental origins of health and disease: experimental and human evidence of
653 fetal programming for metabolic syndrome. *J Hum Hypertens* 26, 405-419.
- 654 DiTirro, D., Philbrook, A., Rubino, K., and Sengupta, P. (2019). The *Caenorhabditis elegans*
655 Tubby homolog dynamically modulates olfactory cilia membrane morphogenesis and
656 phospholipid composition. *Elife* 8, e48789.
- 657 Dokshin, G.A., Ghanta, K.S., Piscopo, K.M., and Mello, C.C. (2018). Robust genome editing
658 with short single-stranded and long, partially single-stranded DNA donors in
659 *Caenorhabditis elegans*. *Genetics* 210, 781-787.
- 660 Ferkey, D.M., Sengupta, P., and L'Etoile, N.D. (2021). Chemosensory signal transduction in
661 *Caenorhabditis elegans*. *Genetics* 217, iyab004.

- 662 Fielenbach, N., and Antebi, A. (2008). *C. elegans* dauer formation and the molecular basis of
663 plasticity. *Genes Dev* 22, 2149-2165.
- 664 Flavell, S.W., Raizen, D.M., and You, Y.J. (2020). Behavioral states. *Genetics* 216, 315-332.
- 665 Gaglia, M.M., and Kenyon, C. (2009). Stimulation of movement in a quiescent, hibernation-like
666 form of *Caenorhabditis elegans* by dopamine signaling. *J Neurosci* 29, 7302-7314.
- 667 Gems, D., Sutton, A.J., Sundermeyer, M.L., Albert, P.S., King, K.V., Edgley, M.L., Larsen, P.L.,
668 and Riddle, D.L. (1998). Two pleiotropic classes of *daf-2* mutation affect larval arrest,
669 adult behavior, reproduction and longevity in *Caenorhabditis elegans*. *Genetics* 150, 129-
670 155.
- 671 Greer, P.L., Bear, D.M., Lassance, J.M., Bloom, M.L., Tsukahara, T., Pashkovski, S.L., Masuda,
672 F.K., Nowlan, A.C., Kirchner, R., Hoekstra, H.E., *et al.* (2016). A family of non-GPCR
673 chemosensors defines an alternative logic for mammalian olfaction. *Cell* 165, 1734-1748.
- 674 Gruner, M., Grubbs, J., McDonagh, A., Valdes, D., Winbush, A., and van der Linden, A.M.
675 (2016). Cell-autonomous and non-cell-autonomous regulation of a feeding state-dependent
676 chemoreceptor gene via MEF-2 and bHLH transcription factors. *PLoS Genet* 12,
677 e1006237.
- 678 Gruner, M., Nelson, D., Winbush, A., Hintz, R., Ryu, L., Chung, S.H., Kim, K., Gabel, C.V., and
679 van der Linden, A.M. (2014). Feeding state, insulin and NPR-1 modulate chemoreceptor
680 gene expression via integration of sensory and circuit inputs. *PLoS Genet* 10, e1004707.
- 681 Hall, S.E., Beverly, M., Russ, C., Nusbaum, C., and Sengupta, P. (2010). A cellular memory of
682 developmental history generates phenotypic diversity in *C. elegans*. *Curr Biol* 20, 149-155.
- 683 Hall, S.E., Chirn, G.W., Lau, N.C., and Sengupta, P. (2013). RNAi pathways contribute to
684 developmental history-dependent phenotypic plasticity in *C. elegans*. *RNA* 19, 306-319.
- 685 Hallem, E.A., Dillman, A.R., Hong, A.V., Zhang, Y., Yano, J.M., DeMarco, S.F., and Sternberg,
686 P.W. (2011). A sensory code for host seeking in parasitic nematodes. *Curr Biol* 21, 377-
687 383.
- 688 Hanson, M.A., and Gluckman, P.D. (2014). Early developmental conditioning of later health and
689 disease: physiology or pathophysiology? *Physiol Rev* 94, 1027-1076.
- 690 Heisler, L.K., and Lam, D.D. (2017). An appetite for life: brain regulation of hunger and satiety.
691 *Curr Opin Pharmacol* 37, 100-106.
- 692 Hong, M., Ryu, L., Ow, M.C., Kim, J., Je, A.R., Chinta, S., Huh, Y.H., Lee, K.J., Butcher, R.A.,
693 Choi, H., *et al.* (2017). Early pheromone experience modifies a synaptic activity to
694 influence adult pheromone responses of *C. elegans*. *Curr Biol* 27, 3168-3177 e3163.
- 695 Jin, X., Pokala, N., and Bargmann, C.I. (2016). Distinct circuits for the formation and retrieval of
696 an imprinted olfactory memory. *Cell* 164, 632-643.
- 697 Jobson, M.A., Jordan, J.M., Sandrof, M.A., Hibshman, J.D., Lennox, A.L., and Baugh, L.R.
698 (2015). Transgenerational effects of early life starvation on growth, reproduction, and
699 stress resistance in *Caenorhabditis elegans*. *Genetics* 201, 201-212.
- 700 Kaletsky, R., Lakhina, V., Arey, R., Williams, A., Landis, J., Ashraf, J., and Murphy, C.T.
701 (2015). The *C. elegans* adult neuronal IIS/FOXO transcriptome reveals adult phenotype
702 regulators. *Nature* 529, 92-96.
- 703 Kamiyama, D., Sekine, S., Barsi-Rhyne, B., Hu, J., Chen, B., Gilbert, L.A., Ishikawa, H.,
704 Leonetti, M.D., Marshall, W.F., Weissman, J.S., *et al.* (2016). Versatile protein tagging in
705 cells with split fluorescent protein. *Nat Commun* 7, 11046.
- 706 Khan, M., Hartmann, A.H., O'Donnell, M.P., Piccione, M., Pandey, A., Chao, P.-H., Dwyer,
707 N.D., Bargmann, C.I., and Sengupta, P. (2022). Context-dependent reversal of odorant

- 708 preference is driven by inversion of the response in a single sensory neuron type. PLoS
709 Biol *In press*.
- 710 Kim, S.M., Su, C.Y., and Wang, J.W. (2017). Neuromodulation of innate behaviors in
711 *Drosophila*. *Annu Rev Neurosci* 40, 327-348.
- 712 Lanjuin, A., and Sengupta, P. (2002). Regulation of chemosensory receptor expression and
713 sensory signaling by the KIN-29 Ser/Thr kinase. *Neuron* 33, 369-381.
- 714 Lin, K., Dorman, J.B., Rodan, A., and Kenyon, C. (1997). *daf-16*: An HNF-3/forkhead family
715 member that can function to double the life-span of *Caenorhabditis elegans*. *Science* 278,
716 1319-1322.
- 717 Matthews, B.J., McBride, C.S., DeGennaro, M., Despo, O., and Vosshall, L.B. (2016). The
718 neurotranscriptome of the *Aedes aegypti* mosquito. *BMC Genomics* 17, 32.
- 719 McLachlan, I.G., Kramer, T.S., Dua, M., DiLoreto, E.M., Dag, U., Srinivasan, J., and Flavell,
720 S.W. (2022). Diverse states and stimuli tune olfactory receptor expression levels to
721 modulate food-seeking behavior. bioRxiv <https://doi.org/10.1101/2022.04.27.489714>.
- 722 Mukhopadhyay, S., Badgandi, H.B., Hwang, S.H., Somatilaka, B., Shimada, I.S., and Pal, K.
723 (2017). Trafficking to the primary cilium membrane. *Mol Biol Cell* 28, 233-239.
- 724 Nachury, M.V., and Mick, D.U. (2019). Establishing and regulating the composition of cilia for
725 signal transduction. *Nat Rev Mol Cell Biol*, 389-405.
- 726 Neal, S.J., Takeishi, A., O'Donnell, M.P., Park, J., Hong, M., Butcher, R.A., Kim, K., and
727 Sengupta, P. (2015). Feeding state-dependent regulation of developmental plasticity via
728 CaMKI and neuroendocrine signaling. *Elife* 3, e10110.
- 729 Nevitt, G.A., Dittman, A.H., Quinn, T.P., and Moody, W.J., Jr. (1994). Evidence for a peripheral
730 olfactory memory in imprinted salmon. *Proc Natl Acad Sci USA* 91, 4288-4292.
- 731 Nishimura, K., Fukagawa, T., Takisawa, H., Kakimoto, T., and Kanemaki, M. (2009). An auxin-
732 based degron system for the rapid depletion of proteins in nonplant cells. *Nat Methods* 6,
733 917-922.
- 734 Nolan, K.M., Sarafi-Reinach, T.R., Horne, J.G., Saffer, A.M., and Sengupta, P. (2002). The
735 DAF-7 TGF-beta signaling pathway regulates chemosensory receptor gene expression in *C.*
736 *elegans*. *Genes Dev* 16, 3061-3073.
- 737 Ogg, S., Paradis, S., Gottlieb, S., Patterson, G.I., Lee, L., Tissenbaum, H.A., and Ruvkun, G.
738 (1997). The Fork head transcription factor DAF-16 transduces insulin-like metabolic and
739 longevity signals in *C. elegans*. *Nature* 389, 994-999.
- 740 Ow, M.C., Borziak, K., Nichitean, A.M., Dorus, S., and Hall, S.E. (2018). Early experiences
741 mediate distinct adult gene expression and reproductive programs in *Caenorhabditis*
742 *elegans*. *PLoS Genet* 14, e1007219.
- 743 Ow, M.C., Nichitean, A.M., and Hall, S.E. (2021). Somatic aging pathways regulate
744 reproductive plasticity in *Caenorhabditis elegans*. *Elife* 10, e61459.
- 745 Peckol, E.L., Troemel, E.R., and Bargmann, C.I. (2001). Sensory experience and sensory activity
746 regulate chemosensory receptor gene expression in *C. elegans*. *Proc Natl Acad Sci USA*
747 98, 11032-11038.
- 748 Peckol, E.L., Zallen, J.A., Yarrow, J.C., and Bargmann, C.I. (1999). Sensory activity affects
749 sensory axon development in *C. elegans*. *Development* 126, 1891-1902.
- 750 Pool, A.H., and Scott, K. (2014). Feeding regulation in *Drosophila*. *Curr Opin Neurobiol* 29, 57-
751 63.
- 752 Popham, J.D., and Webster, J.M. (1979). Aspects of the fine structure of the dauer larva of the
753 nematode *Caenorhabditis elegans*. *Can J Zool* 57, 794-800.

- 754 Remy, J.J., and Hobert, O. (2005). An interneuronal chemoreceptor required for olfactory
755 imprinting in *C. elegans*. *Science* 309, 787-790.
- 756 Ressler, K.J., Sullivan, S.L., and Buck, L.B. (1993). A zonal organization of odorant receptor
757 gene expression in the olfactory epithelium. *Cell* 73, 597-609.
- 758 Riddle, D.L. (1988). The dauer larva. In *The Nematode Caenorhabditis elegans*, W.B. Wood, ed.
759 (New York: Cold Spring Harbor Laboratory), pp. 393-412.
- 760 Riddle, D.L., and Albert, P.S. (1997). Genetic and environmental regulation of dauer larva
761 development. In *C. elegans II*, D.S. Riddle, T. Blumenthal, B.J. Meyer, and J.R. Priess, eds.
762 (Cold Spring Harbor: Cold Spring Harbor Press), pp. 739-768.
- 763 Riddle, D.L., Swanson, M.M., and Albert, P.S. (1981). Interacting genes in nematode dauer larva
764 formation. *Nature* 290, 668-671.
- 765 Roayaie, K., Crump, J.G., Sagasti, A., and Bargmann, C.I. (1998). The Ga protein ODR-3
766 mediates olfactory and nociceptive function and controls cilium morphogenesis in *C.*
767 *elegans* olfactory neurons. *Neuron* 20, 55-67.
- 768 Ryan, D.A., Miller, R.M., Lee, K., Neal, S.J., Fagan, K.A., Sengupta, P., and Portman, D.S.
769 (2014). Sex, age, and hunger regulate behavioral prioritization through dynamic
770 modulation of chemoreceptor expression. *Curr Biol* 24, 2509-2517.
- 771 Sengupta, P., Chou, J.H., and Bargmann, C.I. (1996). *odr-10* encodes a seven transmembrane
772 domain olfactory receptor required for responses to the odorant diacetyl. *Cell* 84, 899-909.
- 773 Sims, J.R., Ow, M.C., Nishiguchi, M., Kim, K.H., Sengupta, P., and Hall, S.E. (2016).
774 Developmental programming modulates olfactory behavior in *C. elegans* via endogenous
775 RNAi pathways. *eLife* 5, e11642.
- 776 Smith, C.J., and Ryckman, K.K. (2015). Epigenetic and developmental influences on the risk of
777 obesity, diabetes, and metabolic syndrome. *Diabetes Metab Syndr Obes* 8, 295-302.
- 778 Sommer, R.J. (2020). Phenotypic plasticity: from theory and genetics to current and future
779 challenges. *Genetics* 215, 1-13.
- 780 Sural, S., and Hobert, O. (2021). Nematode nuclear receptors as integrators of sensory
781 information. *Curr Biol* 31, 4361-4366.
- 782 Taylor, S.R., Santpere, G., Weinreb, A., Barrett, A., Reilly, M.B., Xu, C., Varol, E., Oikonomou,
783 P., Glenwinkel, L., McWhirter, R., *et al.* (2021). Molecular topography of an entire nervous
784 system. *Cell* 184, 4329-4347.
- 785 Troemel, E.R., Chou, J.H., Dwyer, N.D., Colbert, H.A., and Bargmann, C.I. (1995). Divergent
786 seven transmembrane receptors are candidate chemosensory receptors in *C. elegans*. *Cell*
787 83, 207-218.
- 788 Troemel, E.R., Kimmel, B.E., and Bargmann, C.I. (1997). Reprogramming chemotaxis
789 responses: sensory neurons define olfactory preferences in *C. elegans*. *Cell* 91, 161-169.
- 790 Vassar, R., Ngai, J., and Axel, R. (1993). Spatial segregation of odorant receptor expression in
791 the mammalian olfactory epithelium. *Cell* 74, 309-318.
- 792 Vertiz, J., Carstensen, H., and Hong, R. (2021). Dauer development modulates olfactory
793 behavior. *MicroPubl Biol* 2021, 10.17912/micropub.biology.000479.
- 794 Vidal, B., Aghayeva, U., Sun, H., Wang, C., Glenwinkel, L., Bayer, E.A., and Hobert, O. (2018).
795 An atlas of *Caenorhabditis elegans* chemoreceptor expression. *PLoS Biol* 16, e2004218.
- 796 Webster, A.K., Jordan, J.M., Hibshman, J.D., Chitrakar, R., and Baugh, L.R. (2018).
797 Transgenerational effects of extended dauer diapause on starvation survival and gene
798 expression plasticity in *Caenorhabditis elegans*. *Genetics* 210, 263-274.

- 799 Wexler, L.R., Miller, R.M., and Portman, D.S. (2020). *C. elegans* males integrate food signals
800 and biological sex to modulate state-dependent chemosensation and behavioral
801 prioritization. *Curr Biol* 30, 2695-2706.
- 802 White, P.S., Penley, M.J., Tierney, A.R.P., Soper, D.M., and Morran, L.T. (2019). Dauer life
803 stage of *Caenorhabditis elegans* induces elevated levels of defense against the parasite
804 *Serratia marcescens*. *Sci Rep* 9, 11575.
- 805 Younger, M.A., Herre, M., Ehrlich, A.R., Gong, Z., Gilbert, Z.N., Rahiel, S., Matthews, B.J., and
806 Vosshall, L.B. (2020). Non-canonical odor coding ensures unbreakable mosquito attraction
807 to humans. *bioRxiv* doi.org/10.1101/2020.11.07.368720.
- 808 Zhang, L., Ward, J.D., Cheng, Z., and Dernburg, A.F. (2015). The auxin-inducible degradation
809 (AID) system enables versatile conditional protein depletion in *C. elegans*. *Development*
810 142, 4374-4384.
- 811

812

813 **FIGURE LEGENDS**

814 **Figure 1.** Olfactory responses to a panel of volatile attractants is increased in PD adults.

815 **A)** Cartoon of growth conditions for the generation of control and post-dauer (PD) adults.

816 **B)** Behavioral responses of wild-type control and PD adults to a panel of volatile odorants at the
817 indicated dilutions. Chemotaxis index = (Number of animals at the odorant – number of animals
818 at the diluent ethanol) / (Number of animals at the odorant + number of animals at ethanol). Each
819 dot is the chemotaxis index of a single assay plate containing ~50-300 adult hermaphrodites.
820 Bars represent the mean; error bars are SEM. The behaviors of control and PD animals were
821 assayed in parallel in duplicate; ≥ 3 independent experiments. *, **, *** indicate different at
822 $P < 0.05$, 0.01, and 0.001, respectively (two-tailed Welch's t-test).

823 **C)** Average changes in GCaMP2.2b fluorescence in AWA soma to a 30 sec pulse of 10^{-5} diacetyl
824 in control and PD adults. Shaded regions indicate SEM. $n \geq 16$ animals (1 neuron per animal)
825 each.

826 **D)** Quantification of peak fluorescence intensity changes in AWA soma expressing GCaMP2.2b
827 to a 30 sec pulse of diacetyl at the indicated concentrations. Bars represent mean, error bars are
828 SEM. $n \geq 16$ animals (1 neuron per animal) each. Control and PD adults were examined in
829 parallel over at least three days. ** and *** indicate different at each concentration at $P < 0.01$
830 and 0.001, respectively (two-tailed Welch's t-test); ns – not significant.

831

832 **Figure 2.** Ciliary ODR-10 levels are increased in PD adults.

833 **A)** Representative images of AWA neurons expressing *odr-10::t2A::mNeonGreen* from the
834 endogenous *odr-10* locus in control and PD adults. Arrows indicate AWA cell bodies. Anterior is
835 at left. Scale bars: 5 μm .

836 **B)** Quantification of ODR-10::t2A::mNeonGreen fluorescence in AWA soma in control and PD
837 adults. Each dot is a measurement from an individual neuron. Bars represent the mean; error bars
838 are SEM. $n \geq 39$ neurons (≥ 21 animals). Control and PD adults were imaged in parallel on the
839 same day; ≥ 3 independent experiments. ns – not significant.

840 **C)** Representative images of ODR-10::splitGFP₁₁ expression in AWA cilia of control and PD
841 adults also expressing *gpa-4Δ6p::splitGFP₁₋₁₀*. MKS-5::tagRFP marks the ciliary transition
842 zones. Arrows indicate the ciliary base. Anterior is at top. Scale bars: 5 μm.

843 **D)** Quantification of total ciliary ODR-10::splitGFP₁₁ fluorescence in AWA cilia base and
844 primary stalk in control and PD adults also expressing *gpa-4Δ6p::splitGFP₁₋₁₀*. Each dot is a
845 measurement from an individual animal. Bars represent the mean, error bars are SEM. $n \geq 29$
846 animals. Control and PD adults were imaged in parallel; ≥ 3 independent experiments. ***
847 indicates different at $P < 0.001$ (two-tailed Welch's t-test).

848 **E)** Behavioral responses of wild-type control and wild-type control animals overexpressing
849 ODR-10::tagRFP under the *gpa-4Δ6* promoter (OX ODR-10; 5 ng/μl) to the indicated dilutions
850 of diacetyl. Each dot represents the chemotaxis index of a single assay plate containing ~50-300
851 adult hermaphrodites. Bars represent the mean; error bars are SEM. A subset of control and
852 experimental chemotaxis assays were performed in parallel over at least three days. * and **
853 indicate different at each concentration at $P < 0.05$ and < 0.01 , respectively (two-tailed Welch's t-
854 test).

855 **F)** Quantification of peak fluorescence intensity changes in AWA to a 10 sec pulse of 10^{-7}
856 diacetyl. Responses of wild-type control animals injected with *gpa-4Δ6p::odr-10::tagRFP* at 5
857 and 30 ng/μl are shown. Bars represent mean, error bars are SEM. $n \geq 16$ animals (1 neuron per
858 animal) each. Animals were examined over two days with the exception of OX ODR-10 (30

859 ng/ μ l). * and ** indicate different at $P < 0.05$ and < 0.01 , respectively (Kruskal-Wallis with
860 Dunn's multiple comparisons test).

861

862 **Figure 3.** Dauer larvae exhibit upregulated *odr-10* expression and enhanced diacetyl responses.

863 **A)** Representative images of AWA neurons in L3 and dauer larvae expressing ODR-

864 10::t2A::mNeonGreen from the endogenous *odr-10* locus. Arrows indicate AWA cell bodies.

865 Anterior is at left. Scale bar: 5 μ m.

866 **B)** Quantification of ODR-10::t2A::mNeonGreen fluorescence in AWA neurons of the indicated

867 animals. Each dot is a measurement from a single neuron. Bars represent the mean; error bars are

868 SEM. $n \geq 31$ neurons; (≥ 18 animals). L3 and dauer larvae were imaged on the same day, ≥ 3

869 independent experiments. *** indicates different between indicated at $P < 0.001$ (two-tailed

870 Welch's t-test).

871 **C)** Representative images of reconstituted ODR-10::GFP expression in AWA cilia of L3 and

872 dauer larvae. MKS-5::tagRFP marks the ciliary transition zones. Arrows indicate the AWA cilia

873 base. Anterior at top. Scale bars: 5 μ m.

874 **D)** Quantification of total reconstituted ODR-10::GFP fluorescence in the AWA ciliary base and

875 primary stalk in L3 and dauer animals. Each dot is a measurement from an individual animal.

876 Bars represent the mean total fluorescence, error bars are SEM. $n \geq 23$ animals. *** indicates

877 different between indicated at $P < 0.001$ (two-tailed Welch's t-test).

878 **E)** Average changes in GCaMP2.2b fluorescence in AWA to a 30 sec pulse of 10^{-5} dilution of

879 diacetyl in control and PD adults, and dauer larvae. Shaded regions indicate SEM. Control and

880 PD adult data are repeated from Figure 1D. $n \geq 16$ neurons (1 neuron per animal).

881 **F)** Quantification of peak fluorescence intensity changes in AWA expressing GCaMP2.2b to a
882 30 sec pulse of 10^{-5} dilution of diacetyl. Each dot is a measurement from a single neuron. Bars
883 represent mean fluorescence, error bars are SEM. $n \geq 16$ neurons (1 neuron per animal). Control
884 and PD adult data are repeated from Figure 1D. * and *** indicate different at $P < 0.05$ and
885 < 0.001 , respectively (one-way ANOVA with Tukey's multiple comparisons test).

886

887 **Figure 4.** DAF-16 FOXO may be partly necessary for upregulation of *odr-10* expression in
888 dauer larvae.

889 **A)** Cartoons of different growth conditions of *daf-2(e1368)* animals expressing *daf-*
890 *16::mNeptune::AID*, *odr-10::t2A::mNeonGreen* and *gpa-4Δ6p::TIR1* with or without 1 mM
891 auxin.

892 **B)** Quantification of mean *odr-10::t2A::mNeonGreen* fluorescence in AWA in animals grown
893 with or without 1 mM auxin in conditions indicated in **Ai-Aiii**. Each point is a measurement
894 from an individual AWA neuron. Bars represent mean fluorescence, error bars are SEM. $n \geq 46$
895 neurons (≥ 23 animals) for dauers; $n \geq 40$ neurons (≥ 22 animals) for adults. Dauer larvae and
896 control and PD adults grown with or without 1 mM auxin were imaged in parallel; 3 independent
897 experiments. *** indicates different between indicated at $P < 0.001$ (two-tailed Welch's t-test); ns
898 – not significant.

899 **C)** Quantification of GFP fluorescence in AWA neurons expressing GFP under 1.0 kb of wild-
900 type or mutant *odr-10* promoter sequences in which a conserved DAF-16 binding site has been
901 mutated (mut) (Wexler et al., 2020). Each point is a measurement from an individual neuron.
902 Bars represent mean fluorescence, error bars are SEM. $n \geq 21$ neurons (≥ 27 animals). ** and

903 *** indicate different at $P < 0.01$ and < 0.001 , respectively (Kruskal-Wallis test with Dunn's
904 multiple comparisons test); ns – not significant.
905 **D)** Quantification of total reconstituted ODR-10::GFP fluorescence in AWA ciliary base and
906 stalk. *mut* indicates animals in which a conserved DAF-16 binding sequence within the
907 endogenous *odr-10* promoter has been mutated. Each dot is a measurement from an individual
908 neuron. Bars represent the mean total fluorescence, error bars are SEM. $n \geq 29$ animals. Control
909 and PD wild-type data are repeated from Figure 2D. *** indicates different at $P < 0.001$ (one-way
910 ANOVA with Tukey's multiple comparison test); ns – not significant.

911
912 **Figure 5.** Gene expression is altered in AWA following passage through the dauer stage.
913 **A)** MA plot showing enrichment and log₂ fold changes of differentially expressed genes in PD
914 vs control whole worm RNA-Seq libraries. The names of a subset of genes from different gene
915 families are indicated. Up- and down-regulated genes were determined by differential expression
916 analysis with a log₂ fold change cut off > 1.5 , $\text{padj} < 0.05$.
917 **B)** Waterfall plot of differentially expressed genes from indicated gene families in control and
918 PD whole animal RNA-Seq data. Up- and down-regulated genes were determined by differential
919 expression analysis with a log₂ fold change cut off > 1.5 , $\text{padj} < 0.05$.
920 **C)** MA plot showing enrichment and log₂ fold changes of differentially expressed genes in PD
921 vs control AWA RNA-Seq libraries. The names of a subset of genes from different gene families
922 are indicated. Up- and down-regulated genes were determined by differential expression analysis
923 with a log₂ fold change cut off > 1.5 , $\text{padj} < 0.05$.

924 **D)** Waterfall plot of differentially expressed genes from indicated gene families in PD vs control
925 AWA RNA-Seq libraries. Up- and down-regulated genes were determined by differential
926 expression analysis with a log₂ fold change cut off > 1.5, padj < 0.05.

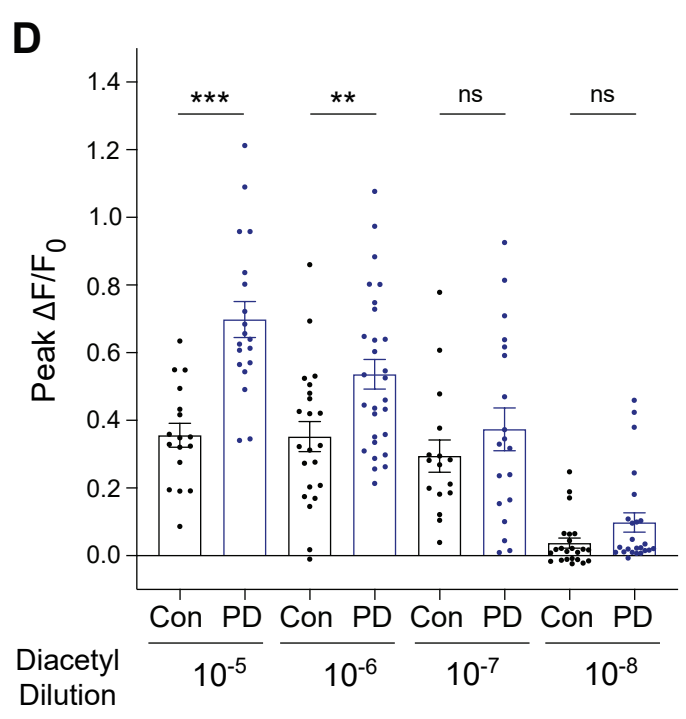
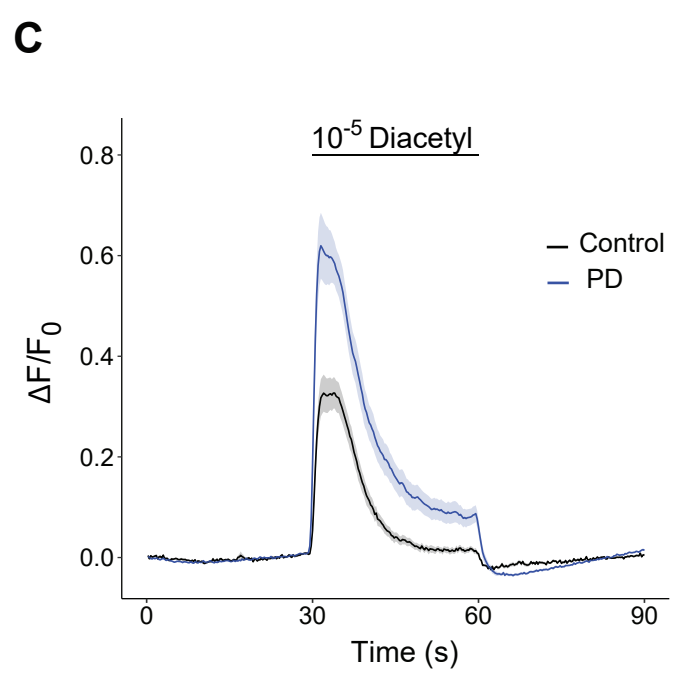
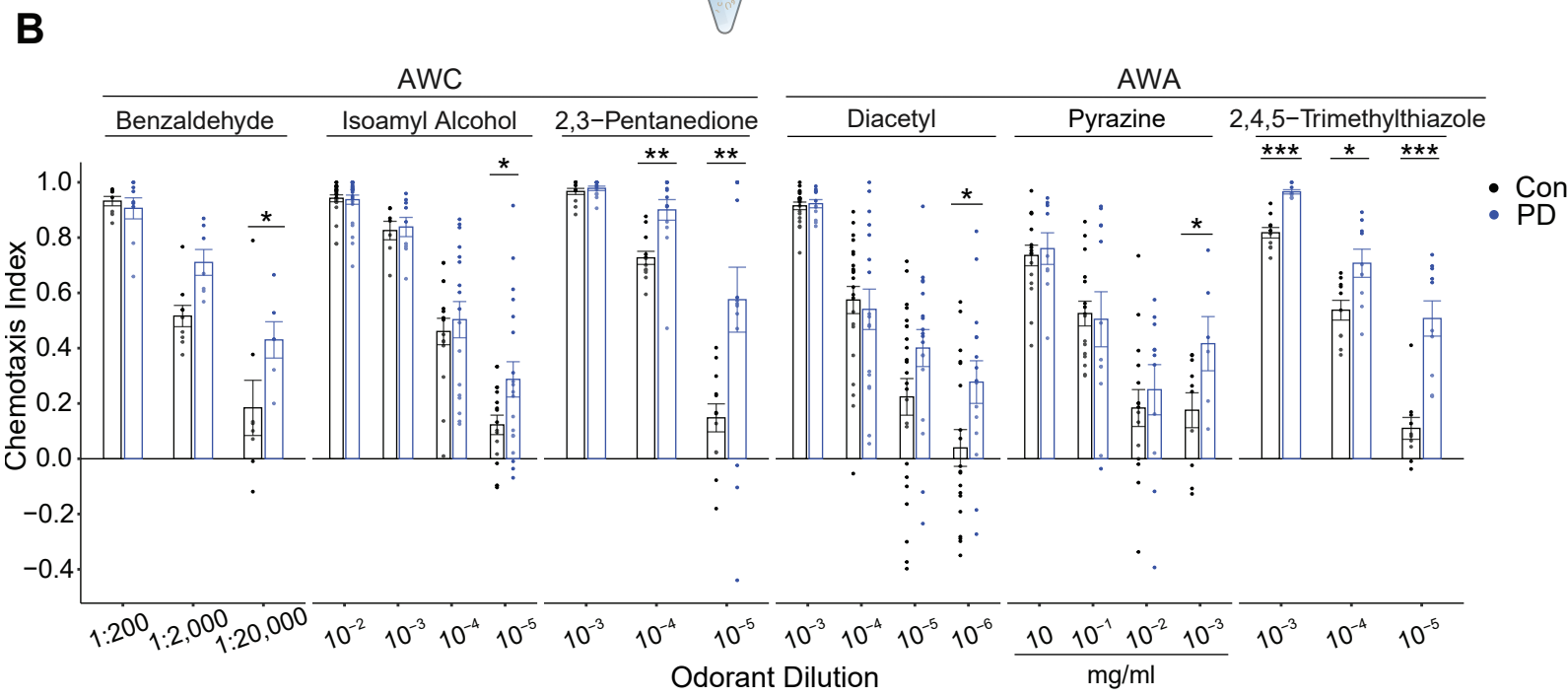
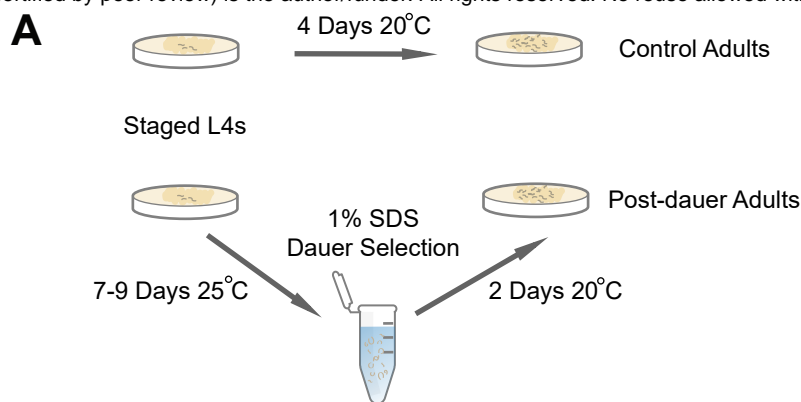
927

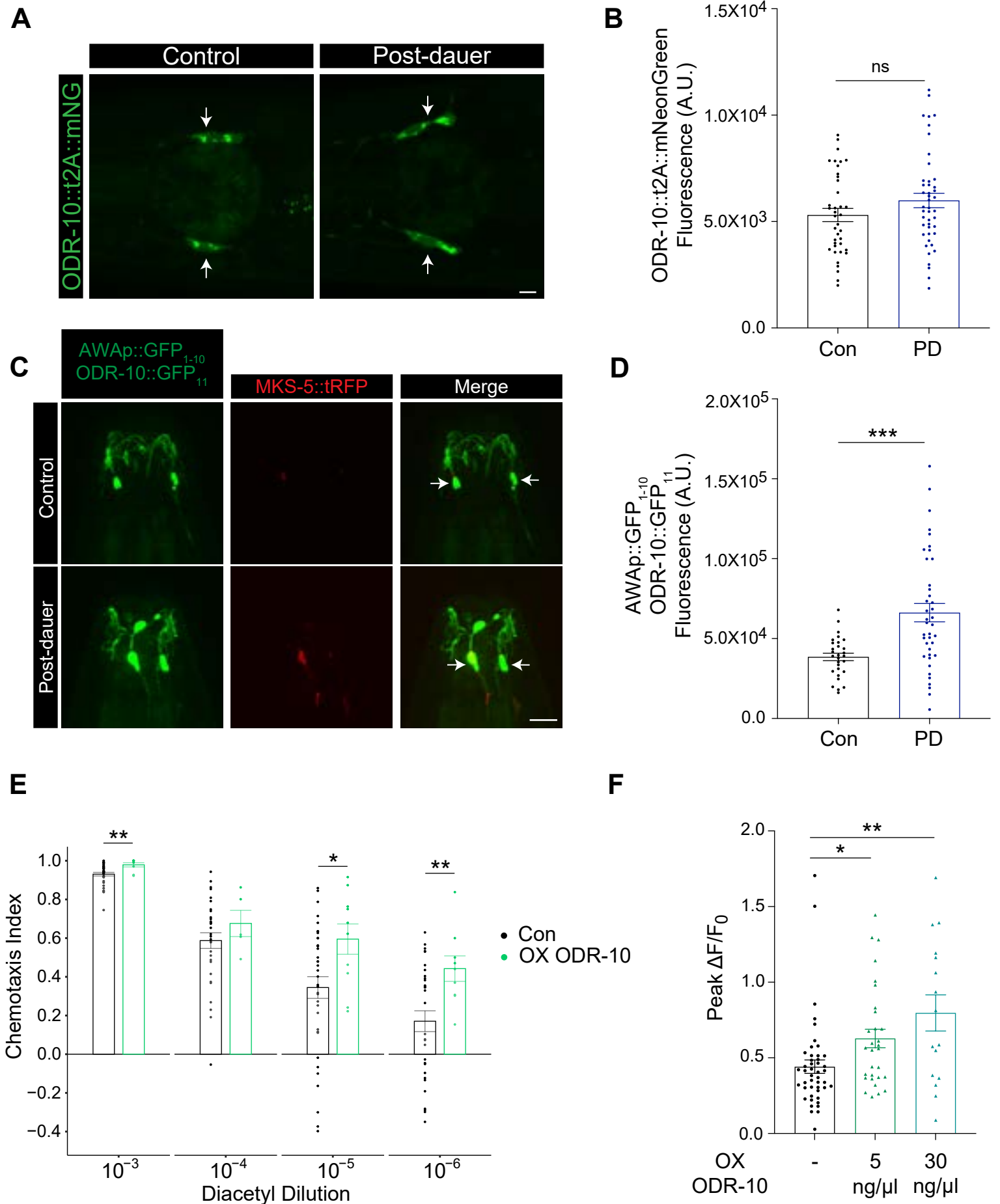
928 **Figure 6.** The expression of a subset of AWA-expressed chemoreceptor genes may be regulated
929 similarly to *odr-10* upon dauer passage.

930 **A)** Representative images of receptor::t2A::mNeonGreen expression from the corresponding
931 endogenous loci in L3, dauer, control, and post-dauer adult stage animals. AWA neurons are
932 marked via expression of *gpa-4Δ6p::tagRFP*. Arrows indicate AWA neurons; asterisks indicate
933 ectopic expression in other cell types. Anterior is at left. Scale bars: 5 μm.

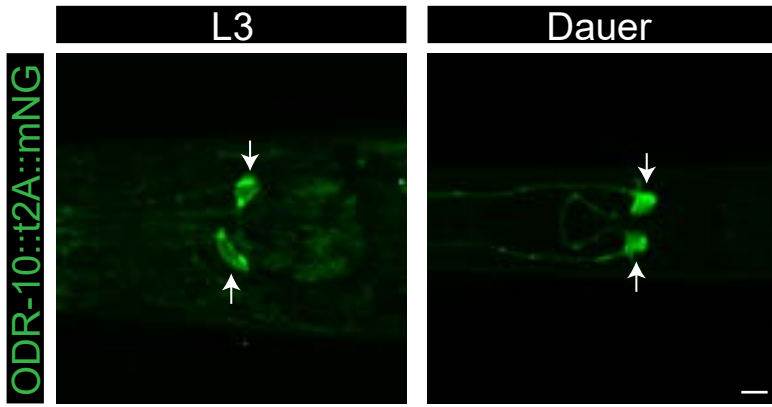
934 **B,C,D)** Quantification of mean receptor::t2A::mNeonGreen fluorescence in AWA neurons in
935 animals of at the indicated developmental stages. Each dot is a measurement from an individual
936 neuron. Bars represent mean; error bars are SEM. $n \geq 28$ neurons (≥ 18 animals). L3 and dauer
937 larvae were imaged in parallel; 3 independent experiments. Control and PD adults were imaged
938 in parallel; 3 independent experiments. *, **, *** indicates different at $P < 0.05$, < 0.01 , and
939 < 0.001 (Kruskal-Wallis with Dunn's multiple comparisons test); ns – not significant.

940 **E)** Quantification of mean SRD-28::t2A::mNeonGreen fluorescence in AWA in *daf-2(e1368)*
941 animals expressing *daf-16::mNeptune::AID* and *gpa-4Δ6p::TIR1* grown with or without 1 mM
942 auxin. Animals were grown as indicated in the cartoon in Figure 4Ai. Each dot is a measurement
943 from an individual neuron. Bars represent mean fluorescence, error bars are SEM. $n \geq 37$
944 neurons (≥ 22 animals). Control and dauers grown on plates with and without 1 mM auxin plates
945 were imaged in parallel; 3 independent experiments. *** indicates different at $P < 0.001$ (two-
946 tailed Welch's t-test); ns – not significant.

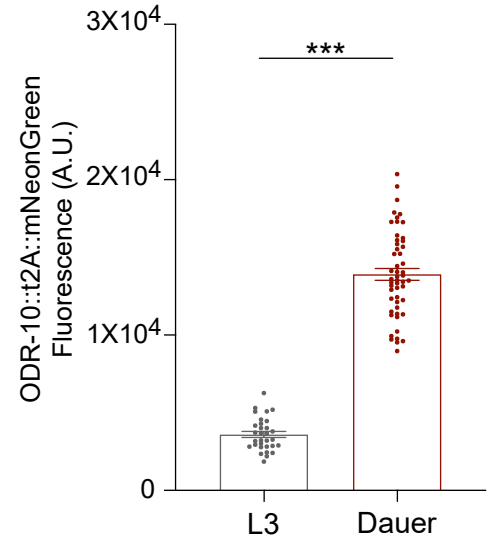




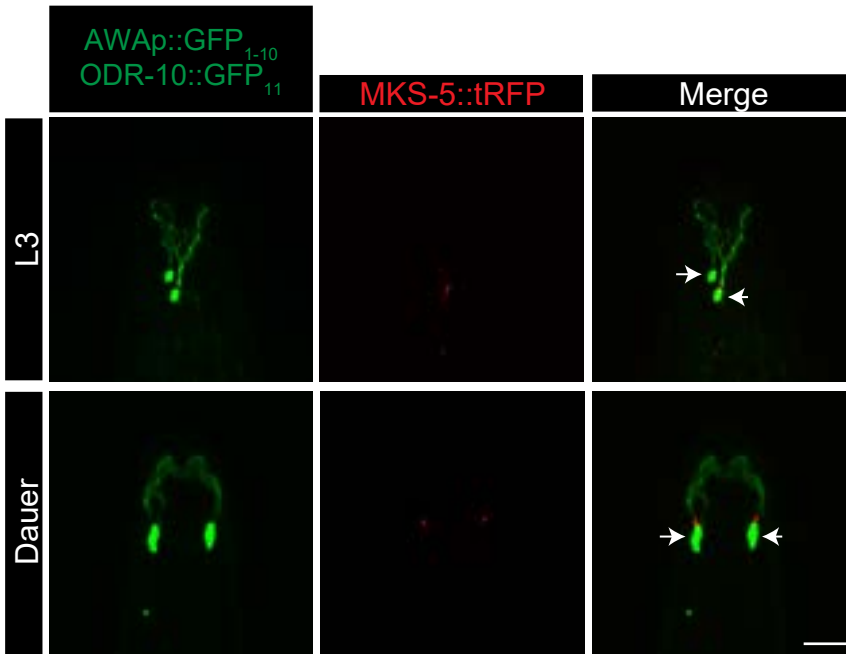
A



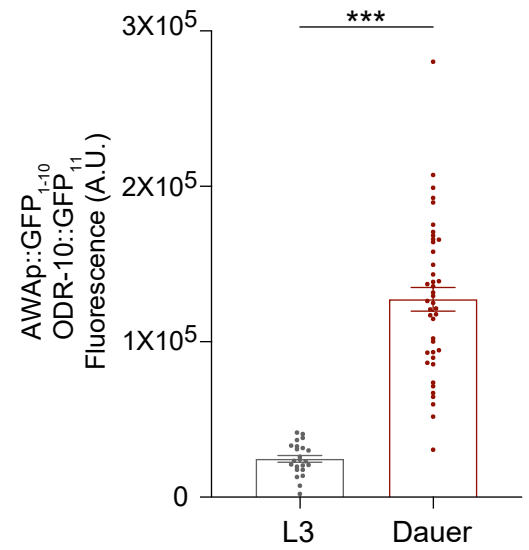
B



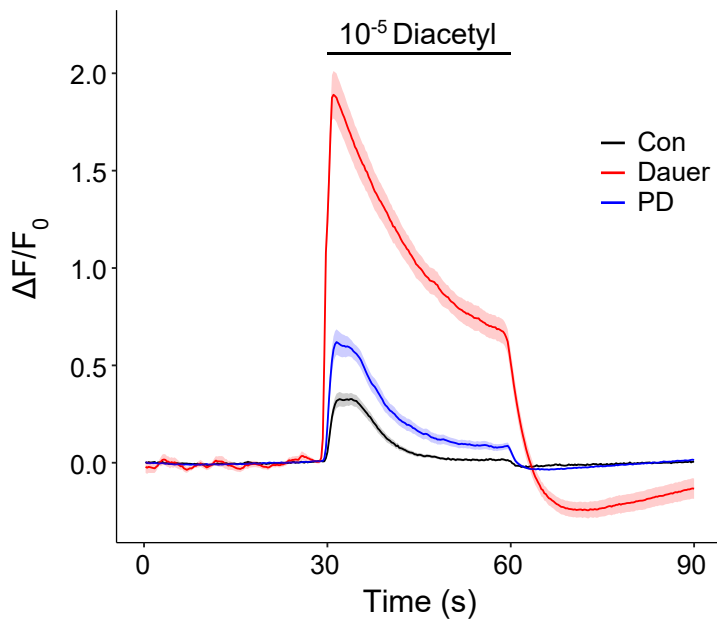
C



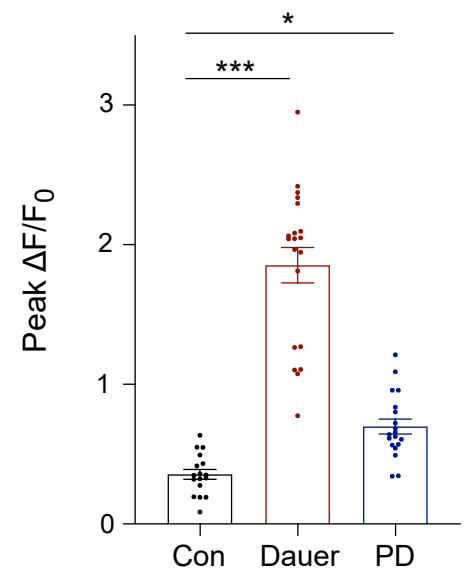
D

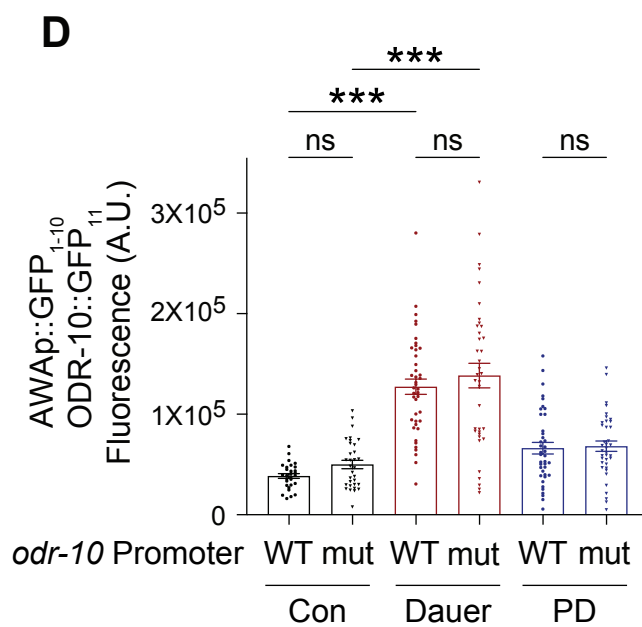
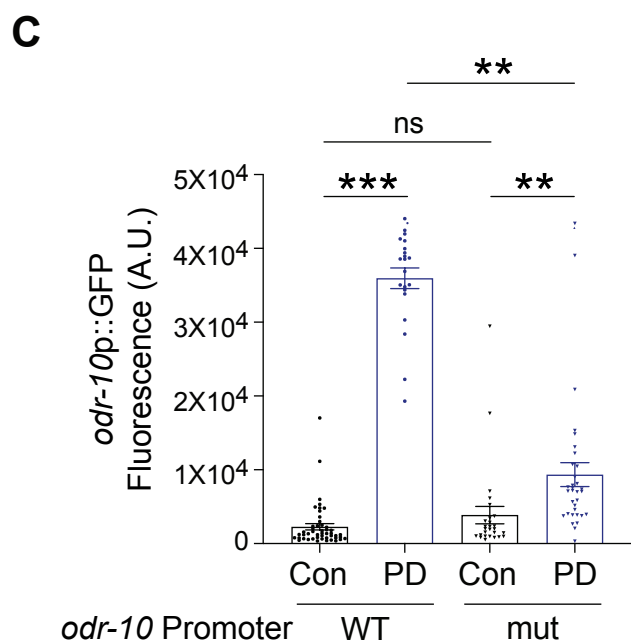
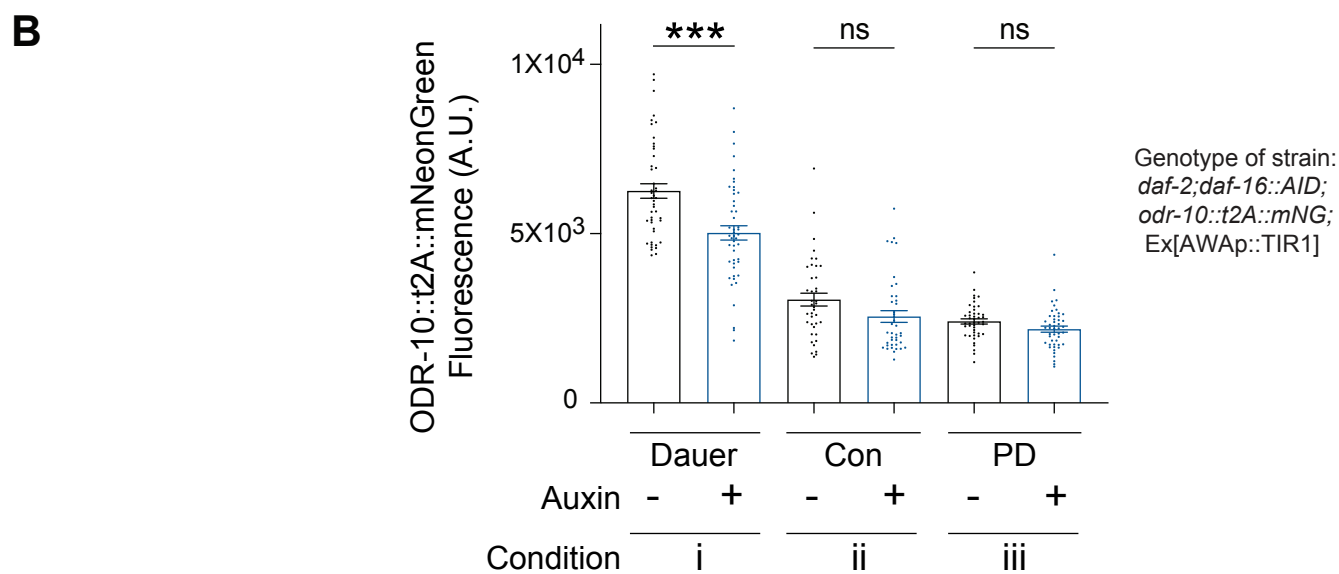
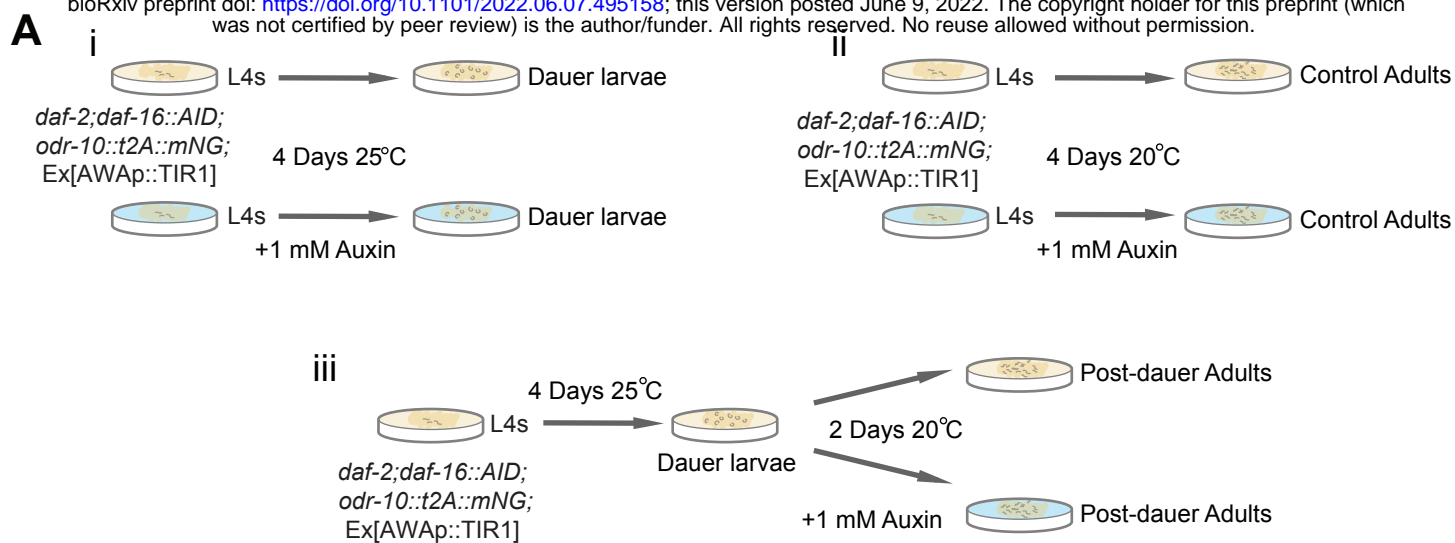


E

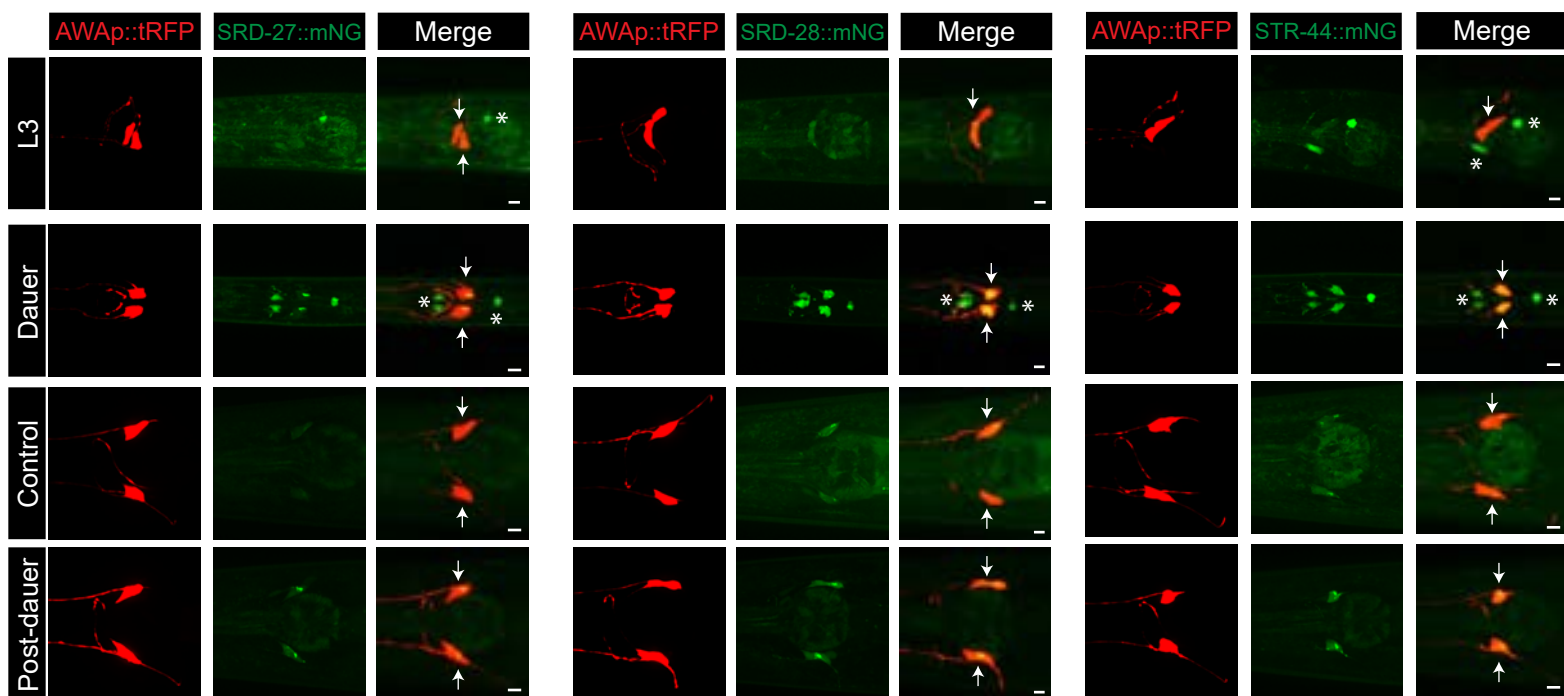


F

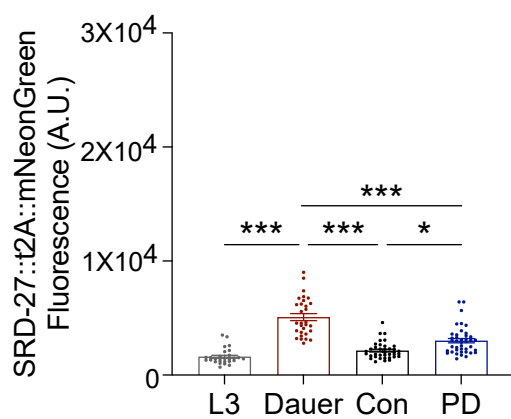




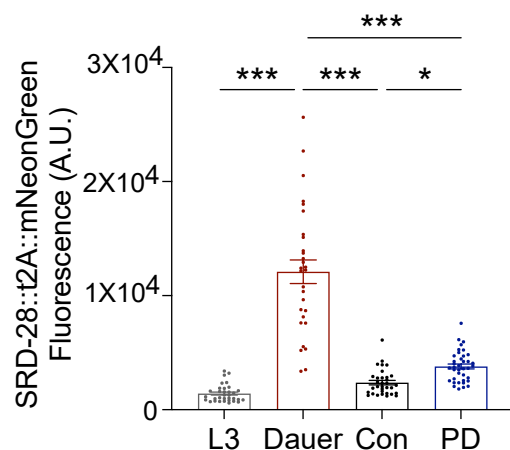
A



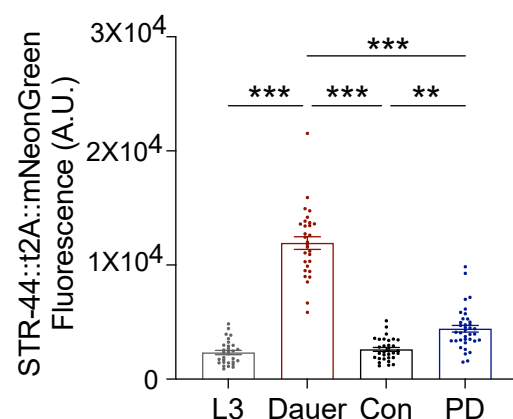
B



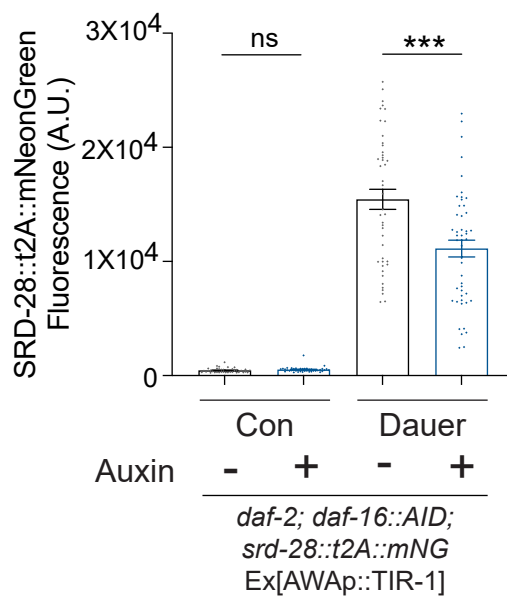
C



D



E



1 SUPPLEMENTAL FIGURE LEGENDS

2 **Figure S1.** Adults that experienced L1 arrest do not exhibit increased diacetyl responses.

3 **A)** Behavioral responses of wild-type control (con) and post-L1 (post-L1 arrest) arrested adults

4 to indicated dilutions of diacetyl. Each dot is the chemotaxis index of a single assay plate

5 containing ~50-300 adult hermaphrodites. Bars represent the mean; error bars are SEM. The

6 behaviors of control and post-L1 arrested animals were assayed in parallel in duplicate; ≥ 3

7 independent experiments; ns – not significant (two-tailed Welch's t-test).

8 **B)** Behavioral responses of wild-type control and PD adults to the indicated concentrations of

9 aversive volatile odorants. Each dot represents the chemotaxis index of a single assay plate

10 containing ~50-300 adult hermaphrodites. Bars represent the mean; error bars are SEM. Control

11 and PD behaviors were assessed in parallel; ≥ 3 independent experiments. * indicates different at

12 $P < 0.05$ (two-tailed Welch's t-test); ns – not significant.

13 **C)** Baseline GCaMP2.2b fluorescence in AWA soma in the indicated wild-type animals.

14 Baseline measurements were collected from experiments reported in Figures 1D and 3F. Each

15 dot is the measurement from a single neuron. Bars represent the mean; error bars are SEM. $n \geq$

16 17 animals (1 neuron per animal). * indicates different at $P < 0.05$ (one-way ANOVA with

17 Tukey's multiple comparisons test); ns – not significant.

18

19 **Figure S2.** An endogenously tagged *odr-10::gfp11* strain retains dauer passage-dependent

20 olfactory behavioral plasticity as adults.

21 **A)** Behavioral responses of *odr-10(oy158)* control and PD animals expressing *odr-10::gfp11* from

22 the endogenous *odr-10* locus to the indicated dilutions of diacetyl. Each dot represents the

23 chemotaxis index of a single assay plate containing ~50-300 adult hermaphrodites. Bars

24 represent the mean; error bars are SEM. Chemotaxis assays at each concentration were
25 performed in parallel over at least three days. ** and *** indicate different at each concentration
26 at $P < 0.01$ and 0.001 , respectively (two-tailed t-test with Welch's correction).

27 **B)** Average changes in GCaMP2.2b fluorescence in AWA soma in control animals of the
28 indicated genotypes to a 10 sec pulse of 10^{-7} diacetyl. Shaded regions indicate SEM. $n \geq 16$
29 animals (1 neuron per animal) each.

30

31 **Figure S3.** Transcriptional profiling of sorted populations of AWA neurons.

32 **A)** PCA clustering of RNA-Seq libraries from sorted populations of AWA neurons and
33 dissociated cells from whole animals based on the 10,000 most differentially expressed genes.

34 **B)** Tissue Enrichment Analysis with the web-based Tissue Enrichment Analysis tool
35 (<https://www.wormbase.org/tools/enrichment/tea/tea.cgi>) (Angeles-Albores et al., 2016) shows
36 enrichment of AWA-expressed genes in AWA RNA-Seq libraries. \log_2 fold change cut off > 2 ,
37 $\text{padj} < 0.05$.

38 **C)** MA plot showing differentially expressed genes in RNA-Seq data from FACS-sorted
39 populations of control and PD AWA neurons as compared to dissociated but unsorted cells from
40 control and PD whole animals. 20 of the most highly AWA-expressed genes (Taylor et al., 2021)
41 are indicated. Up- and down-regulated genes were determined by differential expression analysis
42 with a \log_2 fold change cut off > 2 , $\text{padj} < 0.05$.

43

44 **File S1.** RNA-Seq data of differentially expressed genes from control and PD whole animals.

45 **File S2.** RNA-Seq data of differentially expressed genes from sorted control and PD AWA
46 neurons.

47 **Table S1.** Plasmids used in this work.

Plasmid	Construct	Source	Relevant Figures
PSAB1144	<i>gpa-4Δ6p::mks-5::rfp</i>	This work	2C, 2D, S2A, 3C, 3D, 4D
PSAB1280	<i>gpa-4Δ6p::gfp₁₋₁₀</i>	This work	2C, 2D, S2A, 3C, 3D, 4D
PSAB1281	<i>gpa-4Δ6p::odr-10::tagRFP</i>	This work	2E, 2F, S2B
PSAB1282	<i>gpa-4Δ6p::tagRFP</i>	This work	6A, 6B, 6C, 6D
PSAB1283	<i>gpa-4Δ6p::tir1::SL2::mScarlet</i>	This work	4A, 4B, 6E

48

49

50 **Table S2.** Strains used in this work.

Strain	Genotype	Source	Relevant Figures
WT	N2 (Bristol)	CGC	1A, 1B, S1A, S1B
CX14887	<i>kyIs598[gpa-6p::GCaMP2.2b, unc-122p::dsRed]</i>	(Larsch et al., 2013)	1C, 1D, 2F, 3E, 3F, S1C, S2B
PHX3508	<i>odr-10(syb3508) (odr-10::t2A::mNeonGreen)</i>	(McLachlan et al., 2022)	2A, 2B, 3A, 3B
PY12004	<i>odr-10(oy158) [odr-10::gfp1]; oyEx681 [gpa-4Δ6p::gfp1-10; gpa-4Δ6p::mks-5::tagRFP, unc-122p::dsRed]</i>	This work; gift from J. Kaplan	2C, 2D, 3C, 3D, 4D, S2A
PY12009	<i>oyEx683 [gpa-4Δ6p::odr-10::tagRFP, unc-122p::gfp] 5 ng/μl</i>	This work	2E
PY12010	<i>oyEx683 [gpa-4Δ6p::odr-10::tagRFP, unc-122p::gfp; kyIs598[gpa-6p::GCaMP2.2b, unc-122p::dsRed] 5 ng/μl</i>	This work	2F, S2B
PY12412	<i>oyEx684 [gpa-4Δ6p::odr-10::tagRFP, unc-122p::gfp; kyIs598[gpa-6p::GCaMP2.2b, unc-122p::dsRed] 30 ng/μl</i>	This work	2F, S2B
PY12400	<i>odr-10(syb3508) (odr-10::t2A::mNeonGreen); daf-2(e1368); daf-16(ot975) [daf-16::mNeptune2.5::AID]; oyEx687 [gpa-4Δ6p::tir1::SL2::mScarlet, unc-122p::dsRed]</i>	This work; (Aghayeva et al., 2020; Aghayeva et al., 2021; McLachlan et al., 2022)	4A, 4B
CX3260	<i>kyIs37 [odr-10p::gfp + lin-15(+)]</i>	(Sengupta et al., 1996)	4C
PY12401	<i>fsEx571 [odr-10p::Δdaf-16::gfp + myo-3p::mCherry] Line 2, 3x backcrossed</i>	(Wexler et al., 2020)	4C
PY12402	<i>odr-10(oy170) odr-10pΔdaf-16; odr-10(oy158); oyEx681 [gpa-4Δ6p::gfp1-10; gpa-4Δ6p::mks-5::tagRFP, unc-122p::dsRed]</i>	This work	4E
PY10421	<i>oyIs88 [gpa-4Δ6p::myrGFP]</i>	(Maurya and Sengupta, 2021)	5A, 5B, 5C, 5D, S3
PY12403	<i>srd-27(syb2465) (srd-27::t2A::NeonGreen); oyEx688 [gpa-4Δ6p::tagRFP, unc-122p::gfp]</i>	(McLachlan et al., 2022)	6A, 6B
PY12404	<i>srd-28(syb2320) (srd-28::t2A::NeonGreen); oyEx688 [gpa-4Δ6p::tagRFP, unc-122p::gfp]</i>	(McLachlan et al., 2022)	6A, 6C
PY12405	<i>str-44(syb1869) (str-44::t2A::NeonGreen); oyEx688 [gpa-4Δ6p::tagRFP, unc-122p::gfp]</i>	(McLachlan et al., 2022)	6A, 6D
PY12406	<i>srd-28(syb2320) (srd-28::t2A::NeonGreen); daf-2(e1368); daf-16(ot975) [daf-</i>	This work; (Aghayeva et al., 2020; Aghayeva	6E

16::mNeptune2.5::AID]; et al., 2021; McLachlan
oyEx687[gpa- et al., 2022)
4Δ6p::tir1::SL2::mScarlet,
unc-122p::dsRed]

51

52

53 **REFERENCES**

54

55 Aghayeva, U., Bhattacharya, A., and Hobert, O. (2020). A panel of fluorophore-tagged *daf-16*
56 alleles. *Micropub. Biol.* *10.17912/micropub.biology.000210*.

57 Aghayeva, U., Bhattacharya, A., Sural, S., Jaeger, E., Churgin, M., Fang-Yen, C., and Hobert, O.
58 (2021). DAF-16/FoxO and DAF-12/VDR control cellular plasticity both cell-
59 autonomously and via interorgan signaling. *PLoS Biol* *19*, e3001204.

60 Angeles-Albores, D., RY, N.L., Chan, J., and Sternberg, P.W. (2016). Tissue enrichment
61 analysis for *C. elegans* genomics. *BMC Bioinformatics* *17*, 366.

62 Larsch, J., Ventimiglia, D., Bargmann, C.I., and Albrecht, D.R. (2013). High-throughput
63 imaging of neuronal activity in *Caenorhabditis elegans*. *Proc Natl Acad Sci USA* *110*,
64 E4266-4273.

65 Maurya, A.K., and Sengupta, P. (2021). *xbx-4*, a homolog of the Joubert syndrome gene
66 FAM149B1, acts via the CCRK and RCK kinase cascade to regulate cilia morphology.
67 *Curr Biol* *31*, 5642-5649.

68 McLachlan, I.G., Kramer, T.S., Dua, M., DiLoreto, E.M., Dag, U., Srinivasan, J., and Flavell,
69 S.W. (2022). Diverse states and stimuli tune olfactory receptor expression levels to
70 modulate food-seeking behavior. *bioRxiv* <https://doi.org/10.1101/2022.04.27.48971>.

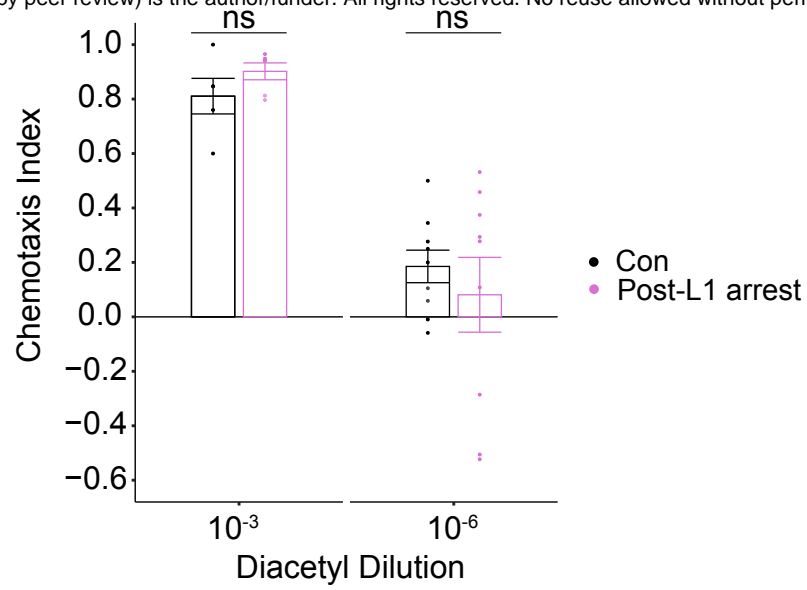
71 Sengupta, P., Chou, J.H., and Bargmann, C.I. (1996). *odr-10* encodes a seven transmembrane
72 domain olfactory receptor required for responses to the odorant diacetyl. *Cell* *84*, 899-909.

73 Taylor, S.R., Santpere, G., Weinreb, A., Barrett, A., Reilly, M.B., Xu, C., Varol, E., Oikonomou,
74 P., Glenwinkel, L., McWhirter, R., *et al.* (2021). Molecular topography of an entire
75 nervous system. *Cell* *184*, 4329-4347 e4323.

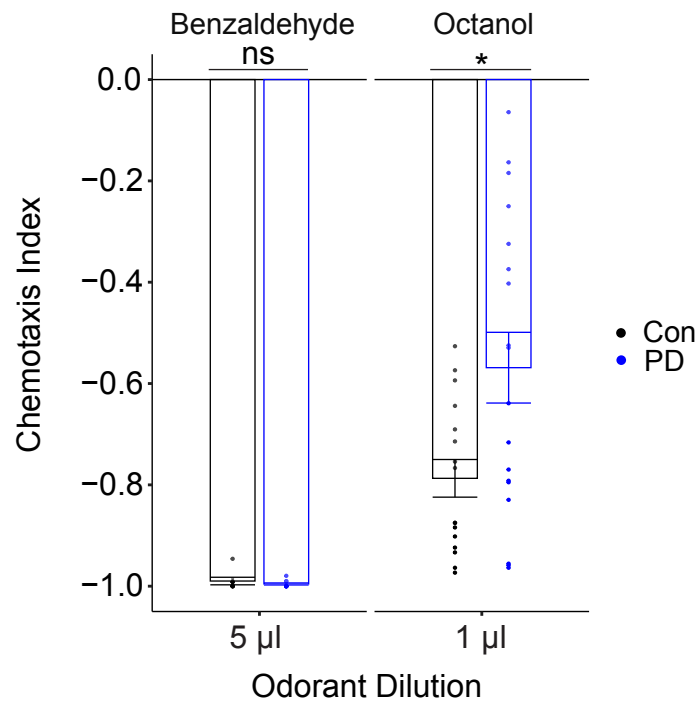
76 Wexler, L.R., Miller, R.M., and Portman, D.S. (2020). *C. elegans* males integrate food signals
77 and biological sex to modulate state-dependent chemosensation and behavioral
78 prioritization. *Curr Biol* *30*, 2695-2706.

79

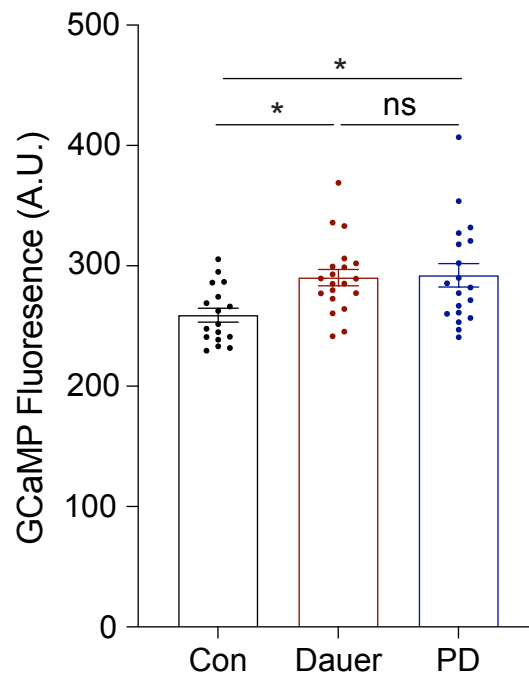
A



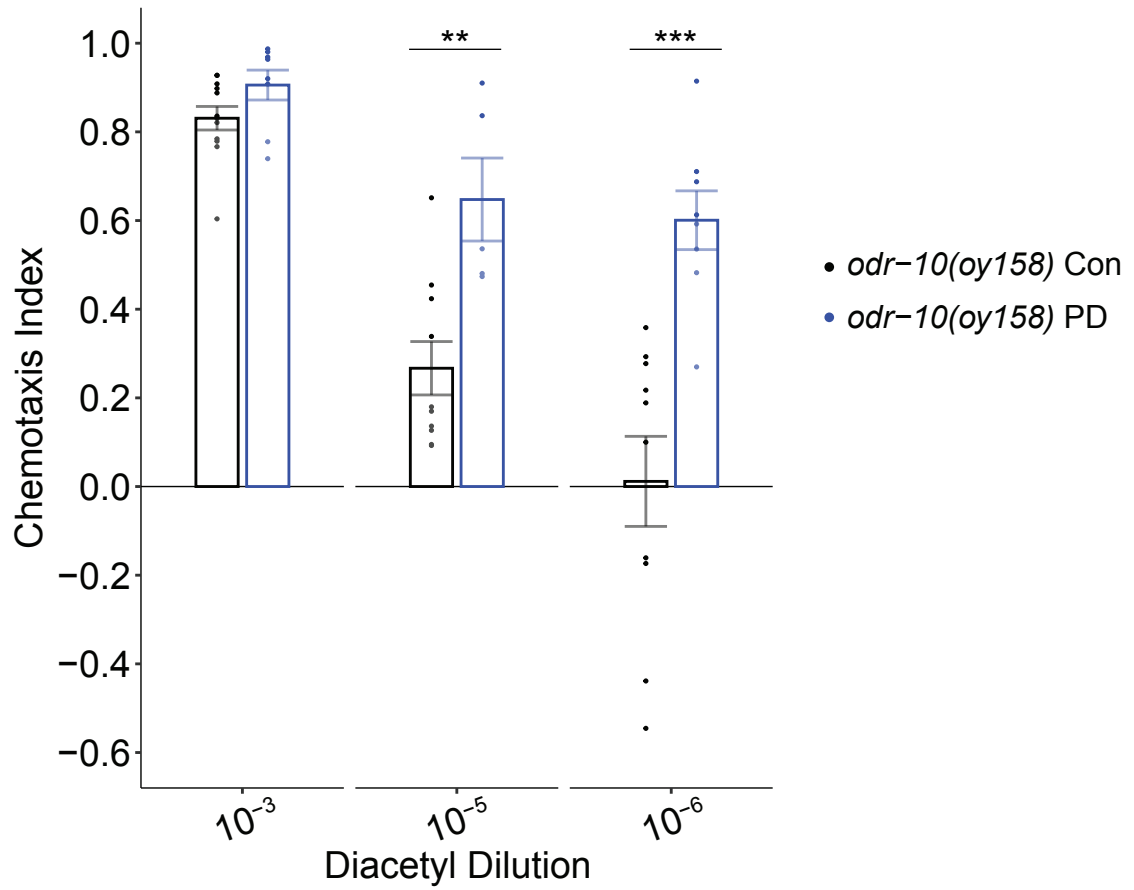
B



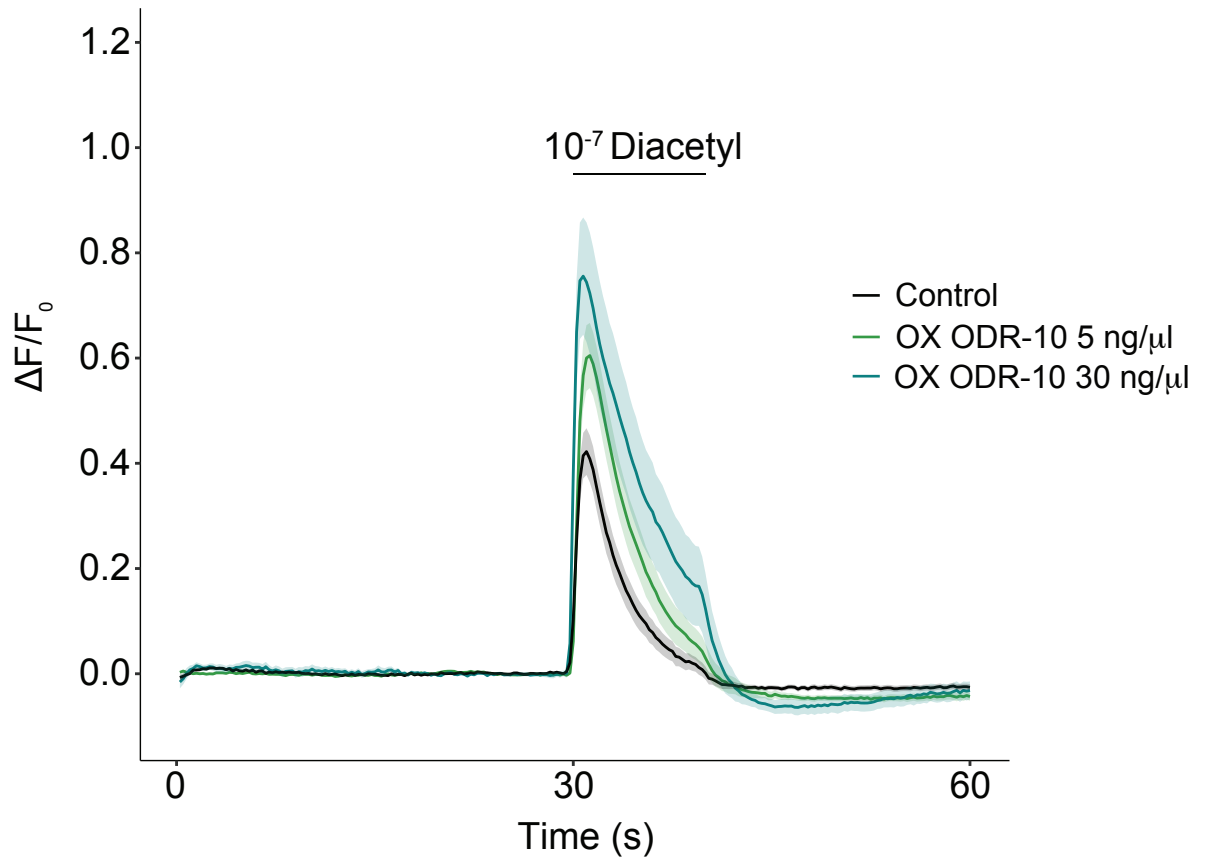
C



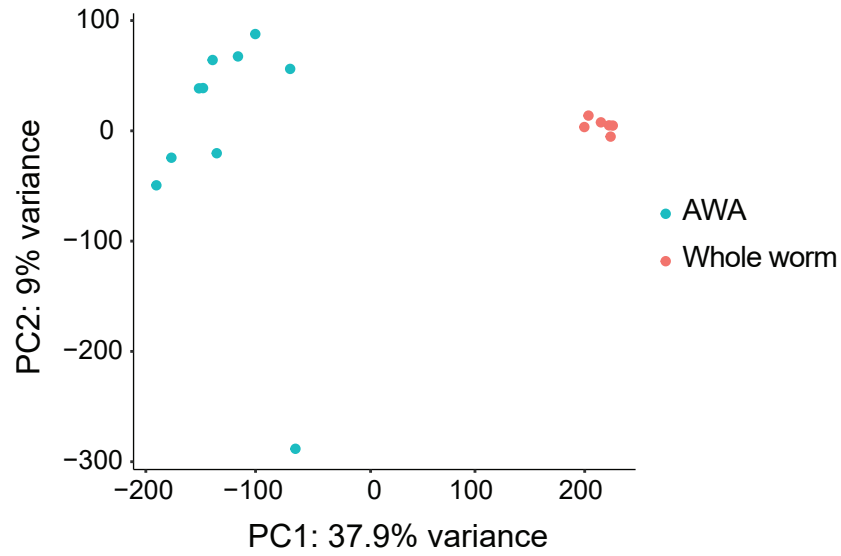
A



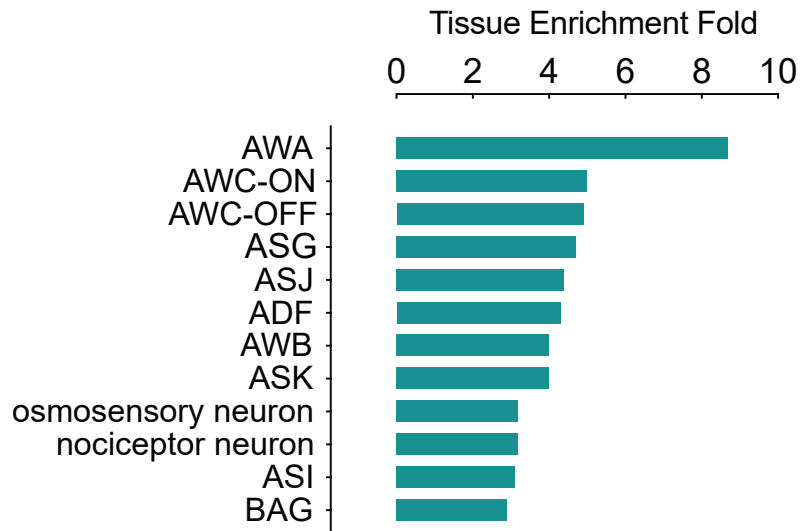
B



A



B



C

